FATIGUE ANALYSIS OF ON-SHORE WIND TURBINE TOWERS

by

Behrouz Badrkhani Ajaei

B.Sc., Civil Engineering, University of Tabriz, 2009

M.Sc., Civil Engineering, University of Tehran, 2012

Submitted to the Institute for Graduate Studies in
Science and Engineering in partial fulfillment of
the requirements for the degree of
Doctor of Philosophy

Graduate Program in Civil Engineering

Boğaziçi University

2020

ACKNOWLEDGEMENTS

I would like to express my deep gratitude to my Ph.D. research supervisor Prof. Serdar Soyöz, for his guidance, support and his encouragement. His continuous support from beginning to the end has made this research possible.

I would like to thank Prof. Hilmi Luş and Assoc. Prof. Barlas Özden Çağlayan for their helpful comments that have played an important role in improvement of quality of this research.

This research was supported by The Scientific and Technological Research Council of Turkey (TÜBITAK) [Grant Number 215M805].

I would like to express my gratitude to Boğaziçi University Foundation (BÜVAK) for their financial support through BÜVAK PhD Scholarship.

Finally, I am thankful to Prof. Emre Otay and Mr. Soner Melih Kural, for providing me access to the recorded sensor data from the wind turbine tower in Saritepe campus of Boğaziçi University.

ABSTRACT

FATIGUE ANALYSIS OF ON-SHORE WIND TURBINE TOWERS

A procedure for estimation of fatigue lives of bolts in flange connections of tubular steel wind turbine towers is developed in this research. The procedure includes numerical calculation of aerodynamic forces, and finite element modeling of the bolted connection. Changes of wind variables are taken into consideration by representative values which are obtained from their probability density functions which are calibrated by wind measurements in the field. Bolt stress time-series calculated numerically and measured by sensors are in agreement in the aspects of fatigue damage and power spectra. The amount of fatigue damage experienced by a bolt is greatly affected by its position in the connection. This procedure uses a limited number of loading cases that represent the long-term variability of the wind parameters, and therefore it requires a reasonable computation effort.

Moreover, the influence of reduction of bolt preload on the fatigue damage experienced by the bolts is evaluated. Results of finite element analyses are used for fatigue calculations. According to the results of this study, loss of bolt preload increases the stress ranges, and consequently increases the fatigue damage. However, this effect is more significant as the bolt preload is reduced to 25 % of the design value.

ÖZET

KARA TİPİ RÜZGAR TÜRBİNİ KULELERİNİN YORULMA ANALİZİ

Bu araştırma boru enkesitli rüzgar türbini kulelerinin bulonlarında yorulma istemlerini hesaplamak için bir yöntem sunmaktadır. Sunulan yöntem aerodinamik yüklerin simulasyonu ve bulonlu bağlantıların yapısal davranışının sonlu elemanlar yöntemiyle modellenmesine dayanmaktadır. Rüzgar parametrelerinin değişkenliği sahadaki ölçümlerle ayarlanan olasılık dağılımlarından elde edilen değerlerle temsil edilmektedir. Sayısal yöntemle oluşturulan gerilme zaman serilerinin, bulonlardaki gerinim ölçerlerden elde edilen ölçümlerle, güç spektrumu ve zaman serileri bakımından uyum gösterdiği belirlenmiştir. Her bulonun pozisyonu o bulonda oluşan yorulma hasarı üzerinde belirleyici bir etkisi vardır. Geliştirilen prosedür, rüzgar değişkenliklerini istatistiksel olarak temsil etmek için sınırlı sayıda simulasyon gerektirmesi nedeniyle, hesaplama açısından verimlidir.

Bu araştırma, ayrıca bulon çekme kuvveti seviyesinin rüzgar türbini bulonlarında oluşan yorulma hasarına etkisini de incelemektedir. Yorulma analizleri, sonlu elemanlar analizlerinin sonuçları üzerinde yapılmıştır. Araştırmanın sonuçları, bulon çekme kuvvetindeki azalmanın gerilme değişimlerinde artışa, ve dolayısıyla yorulma hasarında artışa sebep olduğunu göstermektedir. Bulon çekme kuvvetinin gerilme aralıkları ve yorulma hasarı üzerindeki etkileri, bulon çekme kuvvetinin yaklaşık tasarım çekme kuvvetinin 25 %'ine kadar düştüğünde daha belirgin ve önemli miktarda görünmektedir.

TABLE OF CONTENTS

LIST OF FIGURES

LIST OF TABLES

LIST OF SYMBOLS

A_{Tower}	The cross section area of the tower at a certain height
B_j	The number of the representative values of V_a
B_k	The number of the representative values of TI
d_i	Fatigue damage corresponding to the i'th bin of a histogram
D	Miner's damage index
D_{bolt}	Diameter of the bolt
E	Modulus of elasticity
f_{R}	Rayleigh probability density function
f_W	Weibull probability density function
F_{Axial}	The axial force in a cross section of the tower
F_{bolt}	Bolt preload produced by tightening
F_W	Weibull cumulative distribution function
GPa	Gigapascal
h_{hub}	The height of the turbine hub
$h_{\text{measurement}}$	The height of the wind measurement device
Hz	Hertz
I_{ref}	Reference turbulence intensity
k_b	The stiffness coefficient corresponding to the bolt
k_m	The stiffness coefficient corresponding to the connected members
kN	Kilonewton
K_{nut}	Nut factor
kW	Kilowatt
L	Fatigue life (years)
Ln	Natural logarithm
Log	Logarithm with base 10
Log$N$	Logarithm with base 10 of number of cycles to failure
m	The exponent for the power law wind profile

M_{bending}	The bending moment in a cross section of the tower
mm	Millimeter
MPa	Megapascal
n	The size of the sample set of a random variable
n_i	Number of counted cycles in the i'th bin of a histogram
$n_{i,j}$	The number of counted cycles in the i'th bin of the 1 min long stress range histogram corresponding to the j'th representative value of V_a
$n_{i,j,k}$	The number of counted cycles in the i'th bin of the 1 min long stress range histogram corresponding to the j'th representative value of V_a and the k'th representative value of TI
$n_{i,operational}$	The number of counted cycles in the i'th bin of the yearly operational stress range histogram
$n_{i_{single\ shut-down}}$	The number of counted cycles in the i'th bin of the stress range histogram of a single shut-down event
$n_{i_{single\ start-up}}$	The number of counted cycles in the i'th bin of the stress range histogram of a single start-up event
$n_{i_{shut-down,yearly}}$	The number of cycles in the i'th bin of the yearly shut-down stress range histogram
$n_{i_{start-up,yearly}}$	The number of cycles in the i'th bin of the yearly start-up stress range histogram
N_i	Number of cycles to failure, with a stress range corresponding to the i'th bin of the histogram
$N_{shut-down}$	The yearly number of shut-down events
$N_{start-up}$	The yearly number of start-up events
S_i	Stress range corresponding to the i'th bin of the histogram
$s_{\text{Ln}N_i}$	Standard deviation of LnN_i
$s_{\text{Log}N}$	Standard deviation of Log$N$
S_{Tower}	The elastic section modulus of the tower at a certain height
t_v	Vertical traction
T_{bolt}	Tightening torque applied to the bolt
TI	Turbulence intensity

u_{hub}	Wind speed at hub height
$u_{\text{measurement}}$	The measured wind speed
V	Wind speed
V_a	Short term average of wind speed
V_{ai}	The i'th member of the sample set of V_a
V_{ave}	Long term average of wind speed
$\hat{V}_{ave}$	Estimated value of V_{ave}
W_j	The weighting factor for the j'th representative value of V_a
$W_{j,k}$	The weighting factor for the k'th representative value of TI
X	Any random variable
X_i	The i'th member of the sample set of the random variable X
α	Scale parameter of the Weibull distribution
β	Shape parameter of the Weibull distribution
Γ	The gamma function
ΔP_b	Changes of the bolt load
ΔP_{ex}	Changes of the external load applied to the bolted joint
ΔP_f	Changes of the flange contact force
ζ	Standard deviation of the probability distribution of Ln(TI)
η	The parameter of the Rayleigh probability distribution
$\hat{\eta}$	The estimated value of η
θ	Wind direction angle
μ	Friction coefficient
$\mu_{\text{Ln}(d_i)}$	Mean of natural logarithm of d_i
$\mu_{\text{Ln}(n_i)}$	Mean of natural logarithm of n_i
$\mu_{\text{Ln}(N_i)}$	Mean of natural logarithm of N_i
$\mu_{\text{Ln}(X)}$	Mean of natural logarithm of X
μ_{n_i}	Mean of n_i
μ_{N_i}	Mean of N_i
$\mu_{TI\|V_a}$	Mean of TI for any specific value of V_a
μ_X	Mean of X

$\mu_{\sigma_V \mid V_a}$	Mean of σ_V for any specific value of V_a
ν	Poisson's ratio
$\sigma_{\mathrm{Ln}(d_i)}$	Standard deviation of natural logarithm of d_i
$\sigma_{\mathrm{Ln}(n_i)}$	Standard deviation of natural logarithm of n_i
$\sigma_{\mathrm{Ln}(X)}$	Standard deviation of natural logarithm of X
σ_{n_i}	Standard deviation of n_i
σ_{N_i}	Standard deviation of N_i
$\sigma_{n_{i,assumed}}$	The assumed value of standard deviation of the number of counted cycles in each bin of 1 min long operational histogram or the histograms of single start-up or shut-down events
$\sigma_{n_{i,j}}$	Standard deviation of $n_{i,j}$
$\sigma_{n_{i,j,k}}$	Standard deviation of $n_{i,j,k}$
$\sigma_{n_{i,operational}}$	Standard deviation of $n_{i,operational}$
$\sigma_{n_{i_{shut-down,yearly}}}$	Standard deviation of $n_{i_{shut-down,yearly}}$
$\sigma_{n_{i_{single\ shut-down}}}$	Standard deviation of $n_{i_{single\ shut-down}}$
$\sigma_{n_{i_{single\ start-up}}}$	Standard deviation of $n_{i_{single\ start-up}}$
$\sigma_{n_{i_{start-up,yearly}}}$	Standard deviation of $n_{i_{start-up,yearly}}$
$\sigma_{TI \mid V_a}$	Standard deviation of TI for any specific value of V_a
σ_V	Standard deviation of wind speed
σ_X	Standard deviation of X
$\sigma_{\sigma_V \mid V_a}$	Standard deviation of σ_V for any specific value of V_a
ϕ_{V_a}	Probability density of V_a
ψ	Mean of the probability distribution of $\mathrm{Ln}(TI)$

LIST OF ACRONYMS/ABBREVIATIONS

CDF	Cumulative Distribution Function
FE	Finite Elements
PDF	Probability Density Function

1. INTRODUCTION

Due to the rise of global climate change threat, many nations have adopted a policy of investing in renewable energy production, including production of electricity from wind energy using wind turbines. Unfortunately an ongoing pattern of wind turbine tower collapses is observed around the world, that reduces the financial benefits of investing in the wind energy, and hampers the efforts to promote investment in this industry. Two examples of such tower collapses are [1] and [2].

Wind turbines together with their supporting towers have complex dynamic behavior, and are vulnerable to several types of damage. A categorization of types of structural damage in wind turbines is provided in Chapter 2. However, this research is focused on the subject of fatigue in the connection bolts of wind turbine towers.

This introduction (Chapter 1) describes the objectives of this research, presents an introductory literature review, and specifies the scope of this research.

1.1. Objective

This thesis presents a numerical method of estimating fatigue demands on connection bolts of bolted flange type connections of tubular steel wind turbine towers. The main objective of this research is to present a numerical procedure of fatigue life estimation that takes into consideration the variability of wind and complexities of aero-dynamic loads and bolted connections while it is applicable in the industry. A procedure is developed to take into account the variability of wind speed parameters by sets of wind parameters chosen based on probability distributions of those parameters. Wind load effects on the structure are calculated by coupled aero-dynamic analyses using the FAST [3] software. Internal forces and displacements of the tower calculated by aero-dynamic analyses are applied to the boundaries of a FE model of the bolted connection produced in the ABAQUS [4] software. Walls and flanges of the connec-

tion are modeled by shell elements, and bolts are modeled by beam elements in which preloads are applied by fictitious thermal deformations. Stresses experienced by the bolts are calculated by the FE analyses. Results of the FE analyses show consistency with strain records from strain gauges inside the bolts. The rainflow cycle-counting procedure of ASTM [5] is applied to the calculated stress time-series, and stress range histograms are obtained, which are combined based on the probabilities assigned to different sets of wind parameters. The S-N curve suggested by Eurocode [6] are modified considering the type of the structure and probability of survival, and is used along with the stress range histograms and the Miner's damage index, in order to estimate the average accumulated fatigue damages in a certain time period. Based on the average accumulated fatigue damages, fatigue lives of the bolts are estimated.

This research presents an integrated numerical-experimental framework (summarized in Figure 1.1) for fatigue analysis of wind turbine tower connection bolts. The research presented in this thesis does not determine the safety or quality of products of any specific designer or manufacturer.

Additionally, the effects of loss of preload on fatigue demands imposed on the bolts are investigated.

1.2. Literature Review

Reports of different types of failure, damage and collapse of wind turbines are available in the literature. Ishihara *et al.* [7] reported damages to wind turbines as a result of a typhoon on September 11, 2003. The reported damages include collapses by buckling of two towers, a turbine turning over due to destruction of its foundation, and also cases of breaking of blades and damage to nacelle covers. Ciang *et al.* [8] conducted a literature review and listed failures observed in several parts of wind turbines including breaks, bearings, blades, bolts, hub, generator, gearbox, tower, and anchors. Chou and Tu [1] investigated the collapse of a wind turbine in Taiwan on September 28, 2008. The tower was bent and broken under the effects of a typhoon.

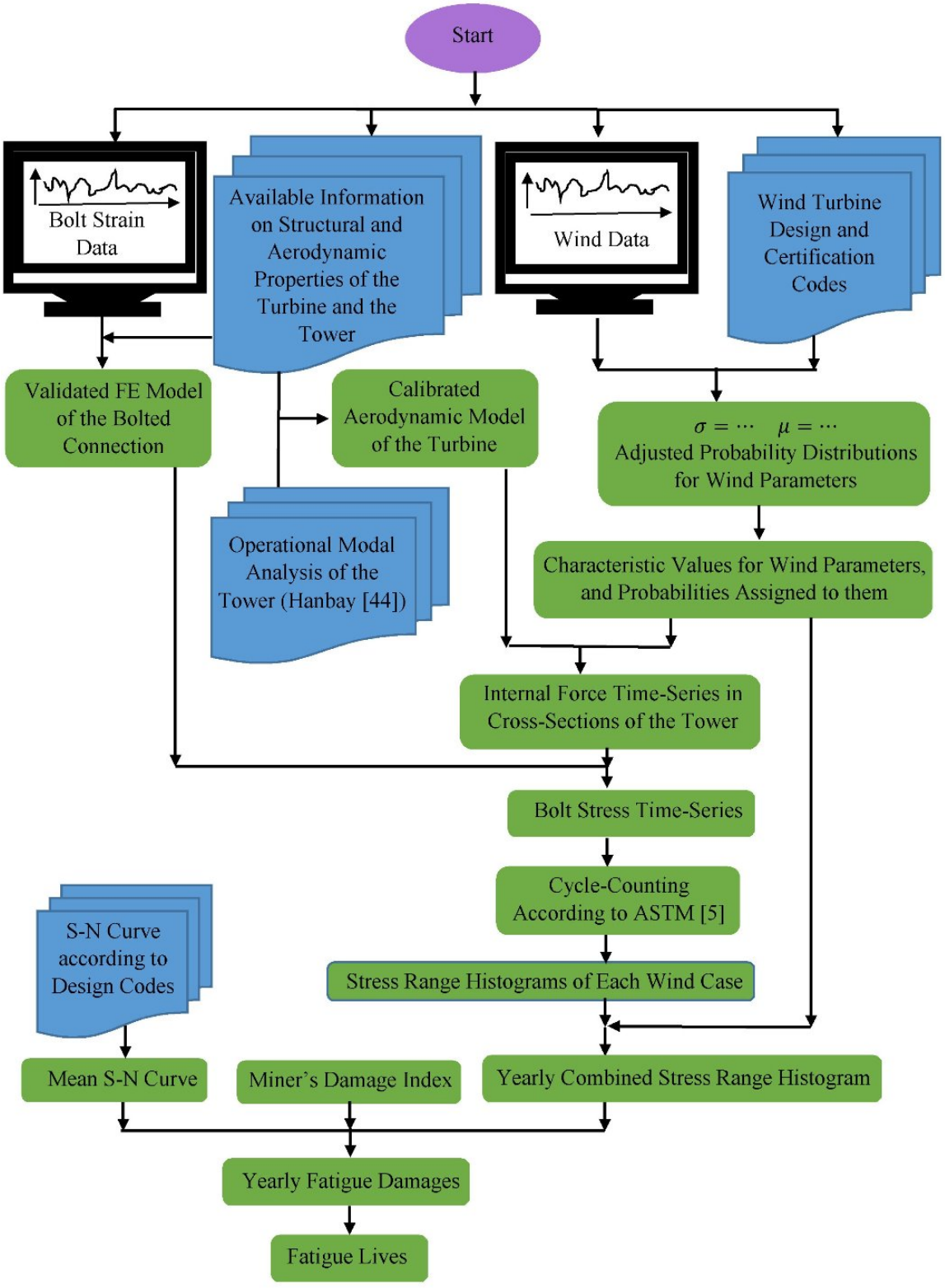

Figure 1.1. The flowchart of the fatigue life estimation procedure

Site investigation of the collapsed turbine tower revealed fractured bolts in the flange connections of the tower. A report of an investigation to a wind turbine collapse in Lemnhult, Sweden, which had happened on December 24, 2015 [2] indicated the occurrence of a fatigue process in the tower bolts before breaking.

In response to the damages and failures observed in wind turbines, extensive research is conducted, focusing on different parts of turbines, different types of failure, and adopting different approaches for design, prediction, monitoring, and prevention. In this section, a brief review of the diverse types of studies on this subject are given.

Sutherland [9] offered a guide for time-domain and frequency-domain fatigue analyses of wind turbines, based on analytic expressions and simplifying assumptions. Similarly, Ragan and Manuel [10] compared time-domain and spectral methods for estimation of wind turbine fatigue loads. Ding and Chen [11] used a probability-based method known as importance splitting to estimate the failure probabilities of wind turbines. Do *et al.* [12] presented an analytical method of obtaining fragility curves for wind turbine towers based on fracture mechanics and structural dynamics. Do *et al.* [13] used the same approach for optimal design of the towers.

Structural health monitoring and modal identification methods are related to the subject of damage in wind turbines from two aspects. Firstly, these methods can diagnose the damages in the structure by comparing the modal properties obtained by monitoring with the modal properties of the undamaged structure. Secondly, modal identification can be used for modal updating of the numerical models used for calculation of structural response and damage. Swartz *et al.* [14] used wireless acceleration sensors for modal identification of three wind turbine towers, and concluded that the data gathered from the sensors had sufficient quality for modal identification. Benedetti *et al.* [15] used strain sensors to monitor the fatigue damage in steel wind turbine tower walls. Pollino and Huckelbridge [16] monitored the fatigue demands on a wind turbine using strain gauges installed on tower wall, over a period of approximately one year. Benedetti *et al.* [17] used classical fracture mechanics to estimate the fatigue life of a

steel wind turbine tower, assuming a crack at the base of the tower.

Research on fatigue and fracture of mechanical parts of wind turbines is outside the scope of this research. However, studying the literature on mechanical parts is useful, since they experience types of loads similar to the tower. Consequently, some of the methods of design and evaluation which are developed for mechanical parts can be used for design and evaluation of damage in towers. Shirani and Harkegard [18] used experimental and statistical methods for determining the fatigue properties of cast iron used in wind turbine components. Fatigue parameters for different types of materials used in gears, blades, bolted joints and other parts of wind turbines are given in [9].

Extensive research is done on behavior of bolted connections, used in wind turbine towers as well as other industries including pressure vessels and pipelines. Literature review on the specific subject of this research, which is fatigue in bolted connections, is provided in Chapter 2.

1.3. Scope

In Chapter 2, types of structural damage in wind turbines are categorized. Subsequently, fatigue in bolts, which is the subject of this research is elaborated. A brief literature review on the specific subject of fatigue in bolts is provided, in continuation of the general literature review in Chapter 1.

Chapter 3 describes the wind turbine at Bogazici university, which is used in this research for a case study.

Chapter 4 presents the general framework developed in this research for fatigue analysis of wind turbine tower connection bolts.

In Chapter 5, effects of preload deficiency on fatigue demands of the wind turbine tower bolts are investigated.

Chapter 6 summarizes the main conclusions of this research.

In Chapter 7 recommendation for future works is given.

2. STRUCTURAL DAMAGE IN WIND TURBINE TOWERS AND THE PROBLEM OF FATIGUE

Wind turbines and their supporting structures experience various types of damage in different parts and components in their lifetimes. In the context of this research, the term "structural damage" refers to the types of damage that would result in partial or complete loss of the capacity of the wind turbine or its supporting structure to support the external loads without collapsing or breaking off of its parts. On the other hand, in this research, the term "non-structural damage" refers to the types of damage that would impede the operation of the turbine, without affecting its structural safety. Damage to various parts of wind turbines is studied in literature, including mechanical parts [18,19], towers [1,12,13,15,16], and blades [20]. This research is interested in the phenomenon of fatigue damage in connection bolts of wind turbine towers.

Due to the cyclic nature of the loads sustained by wind turbine towers, fatigue is a major contributor to structural failures in these towers. Although many other types of structures including bridges are also under the risk of fatigue damage as a result of persistent vibration due to wind loads [21], wind turbine towers are under the influence of multiple sources of load fluctuations, including periodic aerodynamic forces caused by wind shear, effect of wind turbulence, and dynamic effects of mechanical parts [22]. Consequently, fatigue is one of the major subjects covered in wind turbine design and certification codes including [23], and [24]. A report by the Swedish accident investigation authority [2] indicated occurrence of fatigue in bolts as the reason for the tower collapse in Lemnhult. Chou and Tu [1] also report some cases of fatigue damage in wind turbines. In addition to financial losses that may arise from structural failure of wind turbines, human safety is also a concern [25].

Various types of connections have been used in wind turbine towers [26,27]. This thesis focuses on the bolted flange connections, which is a very popular connection type commonly used for tubular wind turbine towers all over the world.

A review of the existing literature in the subject of fatigue in wind turbine towers and the general subject of fatigue reveals that different research projects that are conducted in this subject have adopted different approaches. The approaches and methodologies adopted by researchers can be broadly put into the following three categories: laboratory experiments, in-field measurements or health monitoring, and analytical or numerical studies. However, there may be some research projects that do not fall into these categories, or they may be combinations of two or more of these approaches [28].

Different components of a wind turbine including rotor blades, tower, and mechanical parts may experience fatigue damage. Hamdi and Farah [29] indicate that sustained vibration of the rotor blades can lead to damage in the blades. Shirani and Harkegard [18, 19] investigated fatigue in cast iron material used in wind turbine components. However, fatigue as a type of structural damage is highly sensitive to material and type of loading. While fatigue failure of mechanical components of the turbine results in inability of the turbine to produce power, failure of the connections of the tower may result in collapse and total destruction of the turbine. Due to very large dimensions of wind turbine towers and their connections, full-scale fatigue and fracture experiments on these structures are not practical. Experimental studies in this subject are usually focused on fatigue strength of bolts or small parts of the connection region [30, 31]. One major drawback of these types of experiments is that the loading applied to small parts of the connection in the laboratory may not reflect the complex effects of the aerodynamic loads of the turbine on the bolted connection. Van-Long *et al.* [32] conducted tests on bolted flange plate connections, used in circular tubular structures which are much smaller than connections used in wind turbines, and are subjected to a different type of loading.

In-field measurements and health monitoring is another approach commonly taken by the researchers of this field. Pollino and Huckelbridge [16] obtained stress time histories throughout a year, by in-situ measurements from stain gauges installed on a wind turbine tower. Relying on strain measurements for fatigue life estimation

may be insufficient due to the possibility of missing out special conditions that are statistically likely in the lifetime of the structure, but have not occurred during the measurement period. Benedetti *et al.* [17], suggests a health monitoring scheme of detecting fatigue cracks in bases of the walls of wind turbine towers, by placing numerous strain sensors around the circumference of the tower wall, with small distances between them shorter than the crack length to be detected. The health monitoring approach, though is very useful in understanding the real behavior of the structure, cannot substitute numerical simulation since it requires installing a large number of strain gauges in all the critical points of the structure.

Analytical and numerical methods in addition to being economically more affordable are also very flexible in their capability to take as input many different sets of wind conditions. Therefore, numerical simulation is a necessary part of fatigue analysis of these structures. Analytical and numerical studies have been previously conducted on damage in bolted connections in general. Blachowski and Gutkowski [33] studied the effects of damaged bolted connections on behavior of a telecommunication tower. However, wind turbines have unique aerodynamic behavior that make them different from other structures, and distinguishes this subject from the subject of fatigue in other types of structures.

Numerical procedures commonly used for fatigue design or evaluation of wind turbine towers usually take simplified approaches regarding the local behavior of the critical regions and components where fatigue damage is likely to occur. Do *et al.* [12,13] assumed the fatigue damage occurring in the tower wall at the base of tower. Commonly a linear relationship is assumed between force (or bending moment) and stress (e.g., Annex G of [24]) and cycle-counting is done on force (or bending moment) instead of stress. However, for behavior of complex assemblies like behavior of preloaded bolts in ring-shaped flange connections (which is in the scope of this paper) these types of assumptions are not correct, as it is well-known that in the case of preloaded bolts, only a small portion of changes in external load ranges is transferred to the bolts [34–36].

In order to have accurate estimations of fatigue damage and fatigue life of wind turbine towers, it is essential to have analytical and numerical methods of fatigue analysis that include different aspects of the problem, including aerodynamic-structural interactions of the tower and blades, changes in rotational speed of the rotor, local effects of the geometry and structural details of the connections, and variations of wind speed and turbulence.

3. THE CASE STUDY WIND TURBINE

The case study wind turbine for this research is installed in Saritepe Campus of Bogazici University and is shown in Figure 3.1. It is a 900 kW variable speed on-shore turbine, has a three-bladed upwind rotor, has a rotor diameter of 44 m, and a hub height of 55 m. The steel tower is made of three parts which are shown with different colors

Figure 3.1. A picture of the wind turbine at Bogazici University

in the schematic drawing of Figure 3.2. Bolted connections are used for connecting the parts of the steel tower. Figure 3.2 indicates the position of the bolted connection connecting the middle and lower parts of the tower. The top view of the connection

is shown in Figure 3.3. There are 88 M36 (grade 10.9) bolts in that connection, with a design preload of 510 kN. Figure 3.4 shows the view from the Section A-A of the connection. In this thesis, the positions of the bolts around the circular flange connection are referred to by their clockwise angular positions with respect to North, as shown in Figure 3.3. Bolts positioned at 233^0 and 110^0 positions are instrumented with strain gauges in their shanks. A weather station shown in Figure 3.5 is positioned

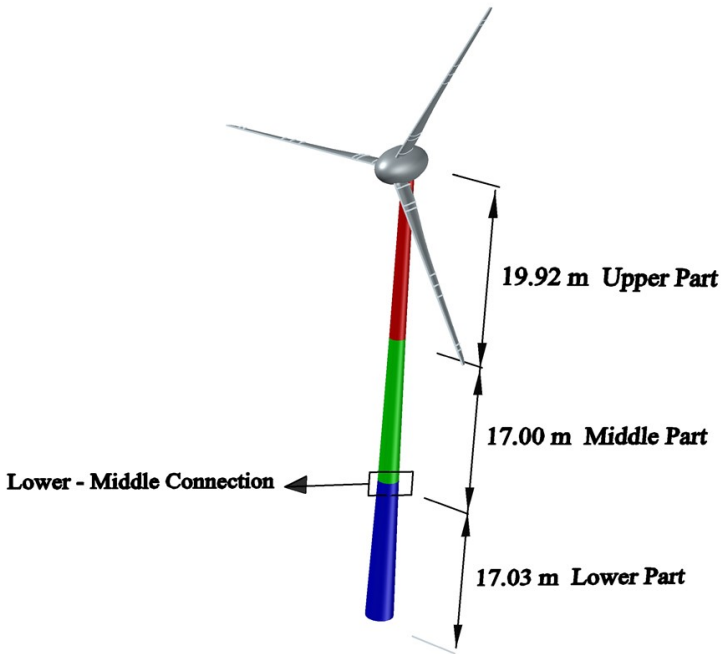

Figure 3.2. Three parts of the steel tower

at a 204 m distance from the tower, in the South-West direction. An ultrasonic device is installed at a height of 60 m from ground, which measures short-term average wind speed (V_a), standard deviation of wind speed (σ_V), and wind direction angle (θ) with respect to North.

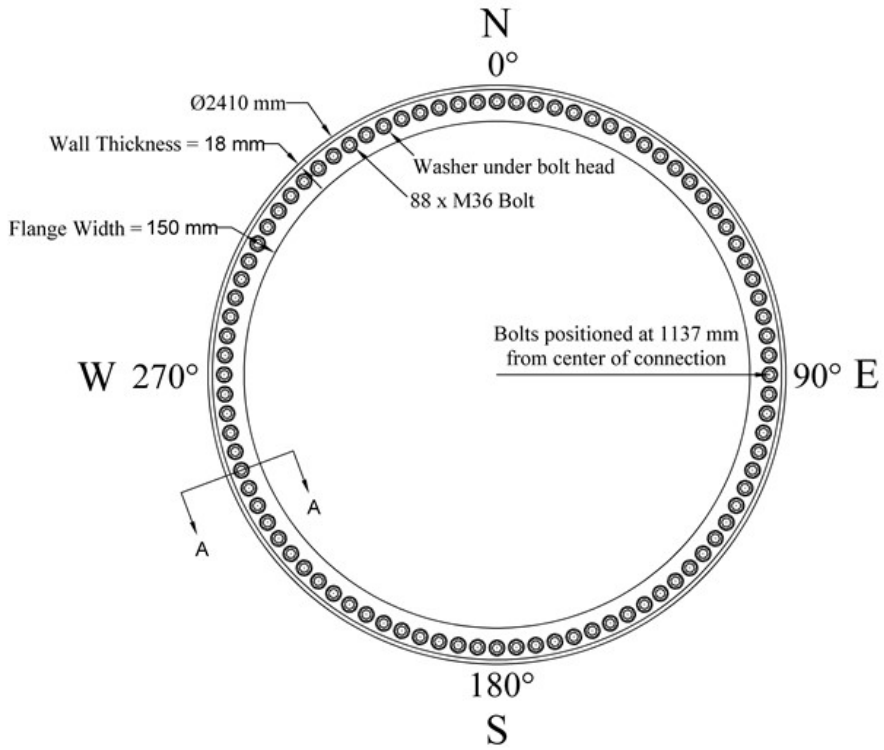

Figure 3.3. Top view of the Lower - Middle connection

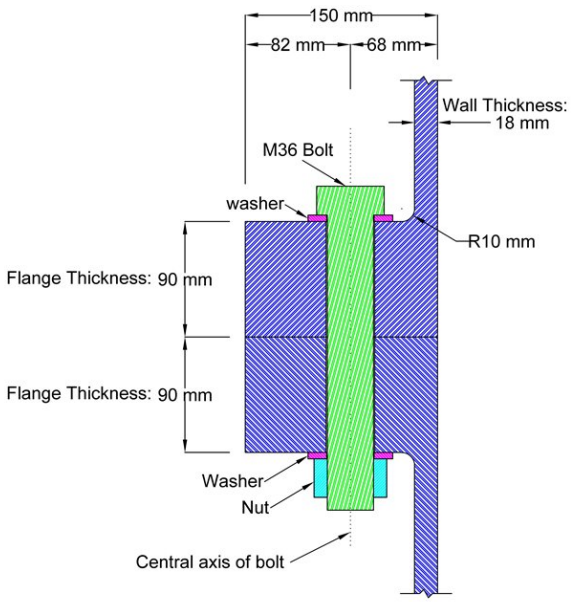

Figure 3.4. View from the Section A-A of the bolted connection

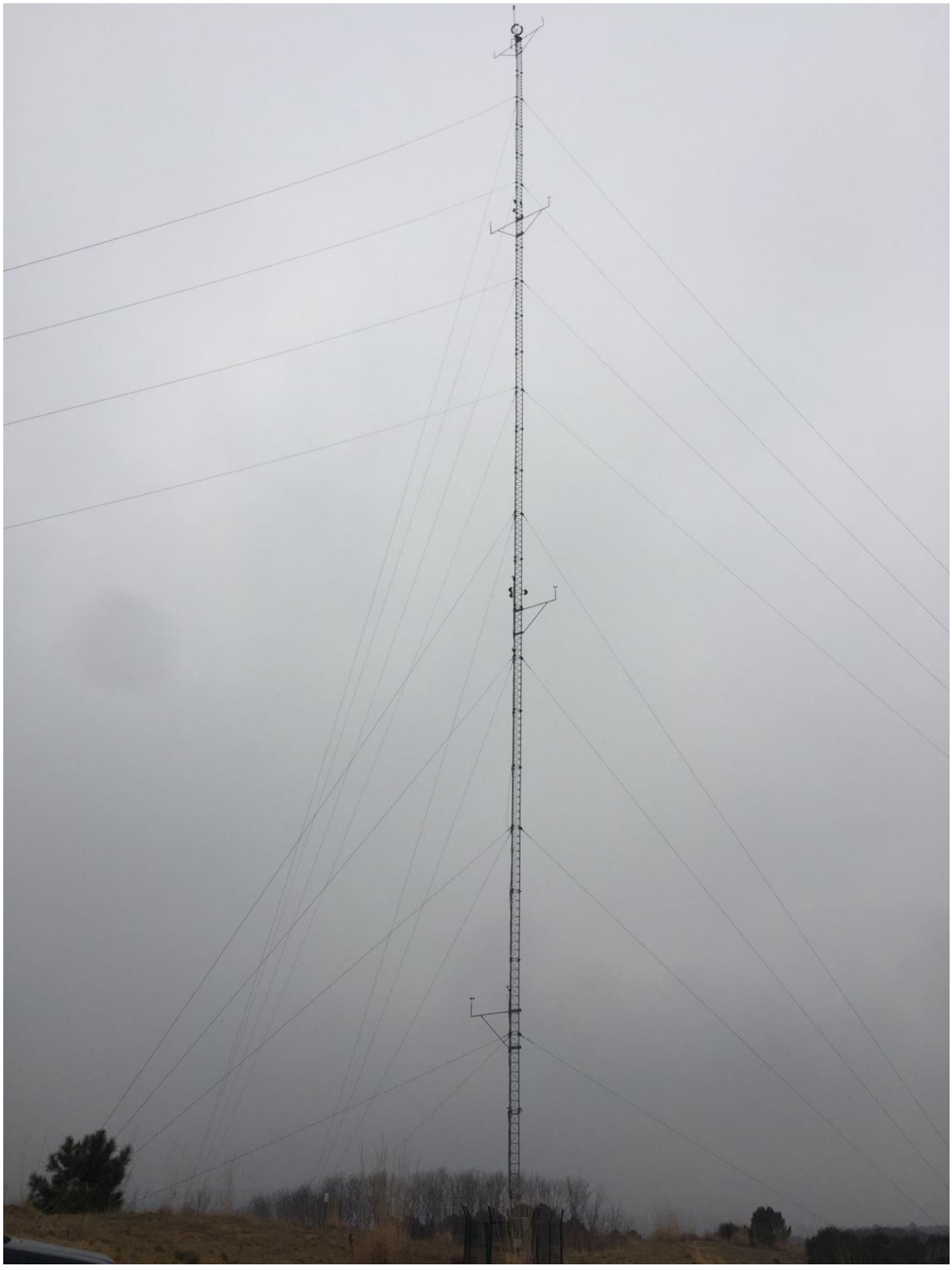

Figure 3.5. The weather station near the wind turbine

4. A GENERAL FRAMEWORK FOR FATIGUE ANALYSIS OF WIND TURBINE TOWER CONNECTION BOLTS

In this chapter, the procedure developed in this research for fatigue analysis of wind turbine tower connection bolts is presented in detail. Though the procedure is presented in the form of a case study of the wind turbine at Bogazici University, it is a general procedure which can be used for similar structures. The results of this chapter are also available in Badrkhani Ajaei and Soyoz [37].

4.1. Simulation of the Aero-Dynamic Loads

Different approaches can be taken to estimate the aerodynamic loads on many types of structures under wind loading, including wind measurements on full-scale structures, small-scale experiments, wind tunnel tests, and numerical simulations [38–40]. In this research, aerodynamic loads on the turbine and the tower are calculated by numerical simulation. As a result of continuous research on wind turbine modeling, methods of numerical analysis of wind turbine towers have evolved from simplified single degree of freedom models to more accurate methods that employ aerodynamic models together with FE models [41]. In this research, the FAST software [3] is used for aerodynamic analyses, which uses the Blade Element Momentum Method for calculating the aerodynamic loads.

Mean wind speed and turbulence intensity are two parameters commonly measured by weather stations and used for characterizing the wind flow in an event or a specific site [42]. In this research, the measurements of these two parameters by the weather station near the wind turbine are used to adjust the parameters of the numerically generated wind speed time-series.

The fatigue analysis performed in this research takes into account the fatigue damage accumulated in the operational conditions, shot-down, and start-up events. Consequently, the aero-dynamic loads applied to the structure in these conditions need to be simulated.

4.1.1. Variations of Wind Parameters

In order to conduct aerodynamic analyses, time series of wind speed are needed. Two major parameters of wind speed time series that affect the fatigue damage are the wind speed average over the time series (V_a), and Turbulence Intensity (TI), defined by Eq. 4.1:

$$TI = \frac{\sigma_V}{V_a} \tag{4.1}$$

where σ_V is the standard deviation of wind speed (V). In this research, Probability Density Functions (PDFs) of these wind parameters are used to choose the values of the wind parameters for which aerodynamic analyses are done. The design guidelines of [24] specify the types of PDFs for the parameters V_a and σ_V, and also provide empirical relationships for the parameters of those PDFs. The relationships given by [24] for estimation of the parameters of PDFs of V_a and σ_V aim to represent a wide range of possible wind turbine sites categorized into a few general categories, which may lead to overly conservative or unsafe estimates for the specific site at which the case-study wind turbine of this research is installed. Therefore, in this study the parameters of the mentioned PDFs are determined using wind measurements recorded by the weather station near the wind turbine.

Based on instructions of [24], a Rayleigh distribution with the Probability Density Function (PDF) as given in Eq. 4.2 can be assumed for variations of wind speed over

an extended period of time.

$$\phi_{V_a}(V_a) = \frac{\pi V_a}{2V_{ave}^2} \exp\left(-\pi\left(\frac{V_a}{2V_{ave}}\right)^2\right) \tag{4.2}$$

where, V_a and V_{ave} denote the short term and long term averages of wind speed respectively.

A set of wind speed measurements are recorded by the weather station between 2015/04/01, 0:00 and 2015/04/02, 23:50. Based on the measurement sample of V_a, and the method explained in Appendix A, the parameter V_{ave} is estimated with the value $\hat{V}_{ave} = 6.86$ m/s.

Figure 4.1 shows the PDF of V_a with the parameter V_{ave} estimated as explained above, where the values that the variable V_a can take in the operational conditions (between the cut-in and cut-out wind speeds) are divided into six intervals separated by boundaries which are shown by dashed vertical lines. In order to represent the variations of wind parameters by a limited number of generated wind speed time series, each one of the V_a intervals in Figure 4.1 need to be represented by a single representative value of V_a. To calculate the representative value of each interval, a weighted average of V_a over each interval is calculated with the probability density (according to Eq. 4.2) used as the weighting factor. Probability of the V_a parameter being inside each interval is calculated by the area under the PDF curve in that interval, and is assigned to the representative value representing that interval. The representative values of V_a and the probabilities assigned to them are shown in Figure 4.1 by a bar diagram.

Standard deviation of the wind speed at hub height over short periods of time (denoted by σ_V) is a random variable in the life time of the turbine. IEC [24] suggests a conditional log-normal probability distribution for σ_V, with mean value and standard deviation as given by Eqs. 4.3 and 4.4.

$$\mu_{\sigma_V|V_a} = I_{ref}\,(0.75V_a + 3.8 \text{ m/s}) \tag{4.3}$$

$$\sigma_{\sigma_V|V_a} = I_{ref}\,(1.4\text{ m/s}) \tag{4.4}$$

where I_{ref} is the reference turbulence intensity, assumed to have a value of 0.16 for the class of the case study wind turbine. However, as illustrated in Appendix B, Eqs. 4.3 and 4.4 are not in agreement with the wind measurements recorded by the weather station. Based on the wind measurements and the procedure explained in Appendix B, Eqs. 4.5 and 4.6 are obtained for mean and standard deviation of TI for any specific value of V_a:

$$\mu_{TI|V_a} = \frac{0.1254V_a + 0.0721}{V_a} \tag{4.5}$$

$$\sigma_{TI|V_a} = \frac{0.48}{V_a} \tag{4.6}$$

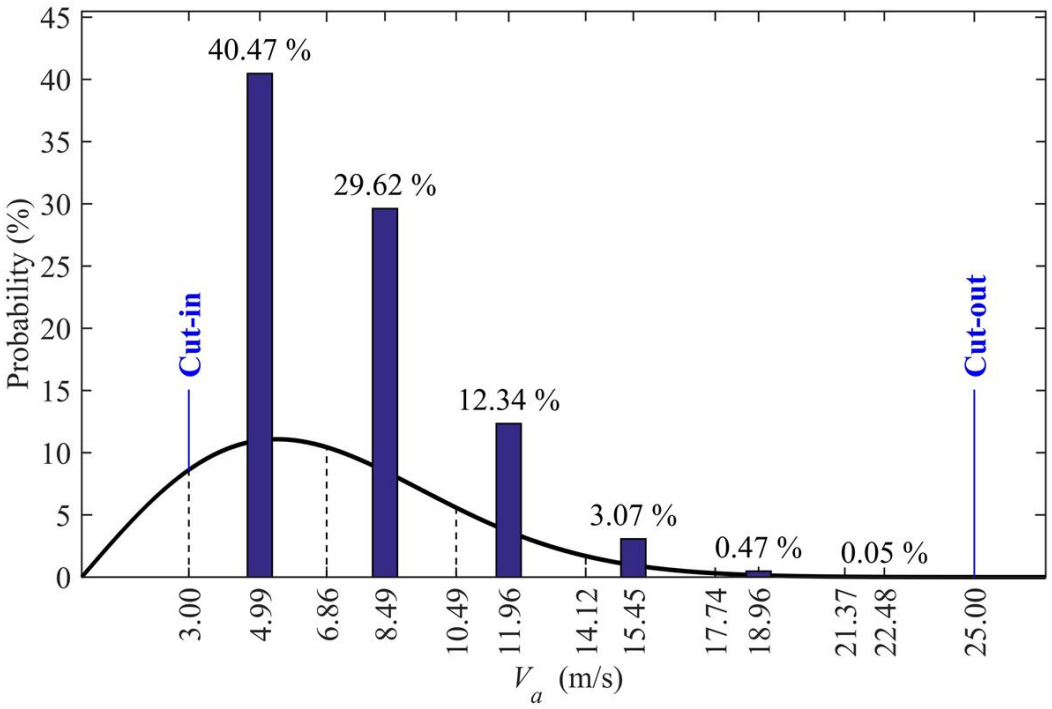

Figure 4.1. PDF and Representative Values of V_a

Using Eqs. 4.5 and 4.6, the parameters of log-normal probability density functions of TI for each representative value of V_a can be calculated. Figure 4.2 shows the PDF of TI for one of those representative values (V_a = 4.99 m/s). The values that the variable TI can take are divided into four intervals, and each interval is represented by a representative value, similar to the approach taken for the V_a parameter. The bar diagram showing the representative values of TI and the probabilities assigned to them is also shown in Figure 4.2.

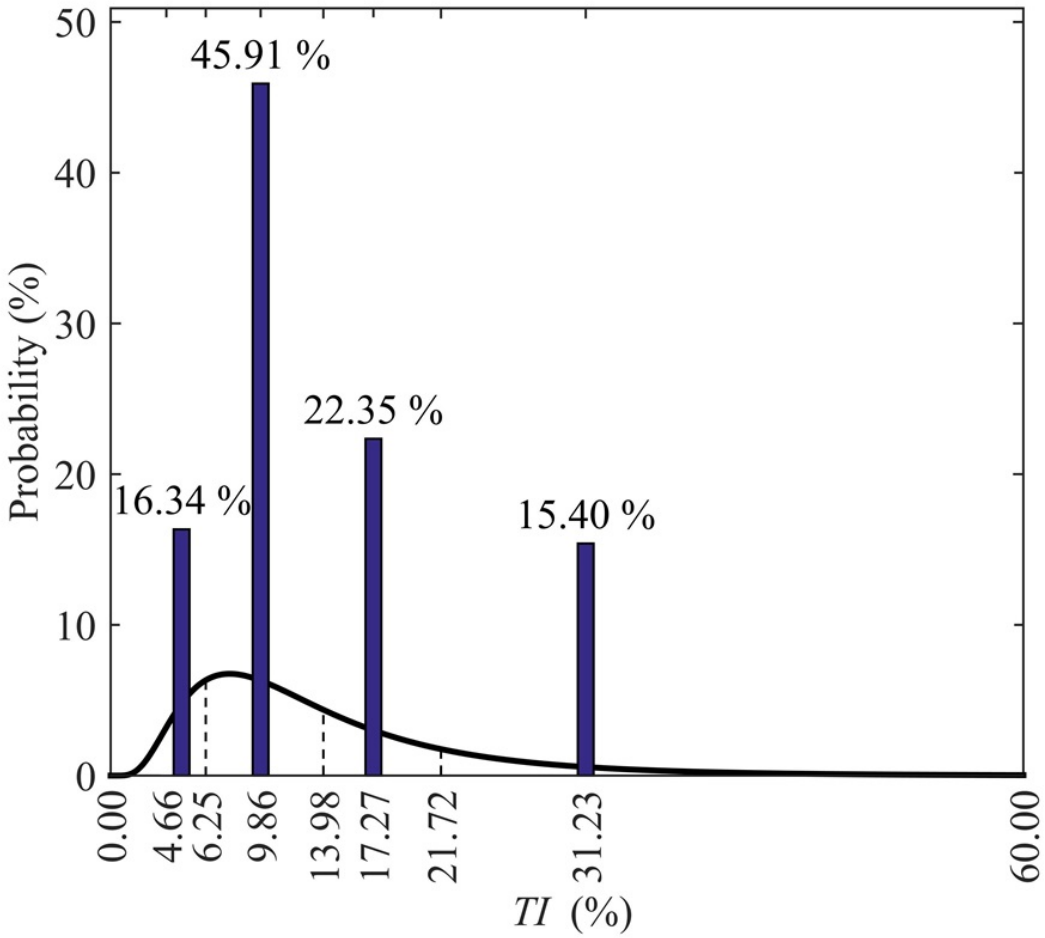

Figure 4.2. PDF and Representative Values of TI for $V_a = 4.99$ m/s

Similarly, for other representative values of V_a, the representative values for TI are obtained with their probabilities of occurrence. For each one of the six representative values of V_a, four representative values of TI are obtained, and consequently, 24 pairs

of (V_a, TI) parameters are chosen as wind cases for the aerodynamic analyses.

The measurement records used for adjusting the wind speed parameters, also include the wind direction measurements. The wind rose shown in Figure 4.3 is plotted based on the measurements of the ultrasonic device of the weather station. The wind rose shows a prevalent wind direction of 202.5^0 from North (Clockwise). Therefore, the rotor disc (together with nacelle) of the wind turbine model is aligned with the prevalent wind direction in the aerodynamic analyses. In the fatigue analyses of this research, the wind direction is assumed to be fixed in the prevalent wind direction. This is a safe approach if the fatigue damage conditions of the most critical bolts are taken as the basis for design and evaluation purposes, and the decisions are applied to all of the bolts equally.

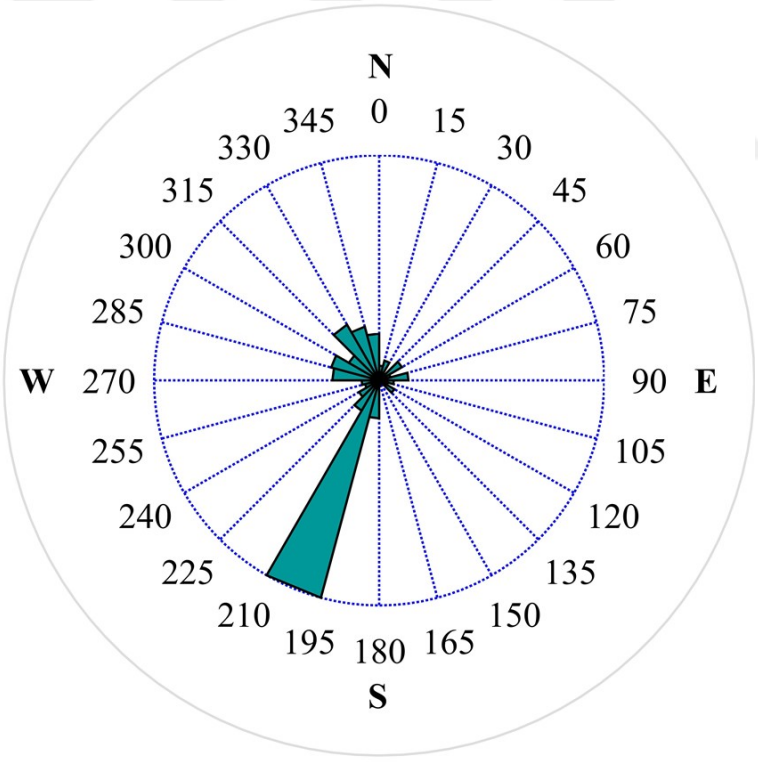

Figure 4.3. Wind rose obtained from measurements

4.1.2. Calculation of the Aero-Dynamic Loads

In this research, the software TurbSim [43] is used to produce time-series of turbulent wind speed. For each set of representative V_a and TI values a wind field time-series is produced. The fields of wind speeds produced by the software TurbSim are used as inputs for aerodynamic analyses of the tower and rotor blades, using the software FAST [3]. The FAST software assumes fixed boundary conditions for the base of the tower. However, due to the soil and foundation flexibility the natural frequencies of a model with rigid base would be higher than the actual natural frequencies of the structure. Hanbay [44] had performed operational modal analysis on 310 days of vibration measurements of the tower studied in this paper. The natural frequencies of the aero-dynamic model used in this paper are adjusted according to the results of the study by Hanbay [44], by adding an extended length of 4.68 m to the base of the tower. Chord lengths of the rotor blades are taken from the values given by the turbine manufacturer. Other aerodynamic and control parameters (such as blade pitch controller and the airfoil shape) of the aerodynamic model are adjusted so that the rotational speed of the model does not exceed the range of rotational speed of the case study turbine (34.5 rpm), and also the power curve obtained by the model roughly fits the power curve of the case study turbine, as shown in Figure 4.4.

Time-series of forces, bending moments and torque in a cross-section of the tower at a distance of 0.414 m above the bolted connection connecting the lower and middle parts of the tower are calculated by the FAST software. Also displacements and rotations in a cross-section 0.304 m below that connection are calculated. Figure 4.5 shows time-series of the major bending moment at the cross-section above the bolted connection for six of the total 24 wind cases (six different sets of V_a and TI values), with the turbine in the operating mode. The differences between the bending moment time-series at different wind speeds originate from several factors including the dependency of the aerodynamic forces on wind speed and the interferences of turbine control systems in higher wind speeds.

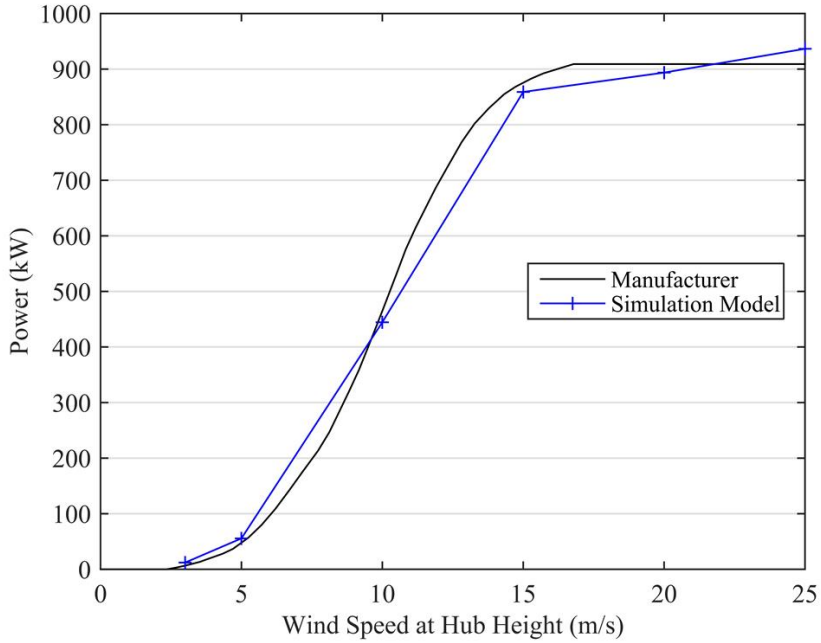

Figure 4.4. Power curve obtained by the model vs. power curve of the case study turbine

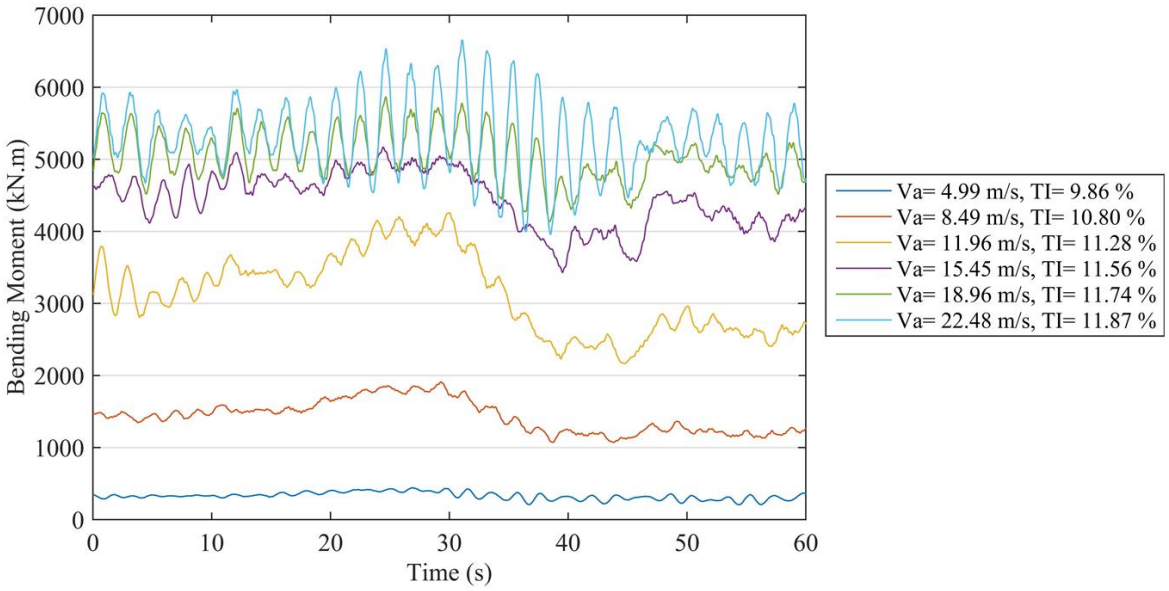

Figure 4.5. Major bending moment above the connection calculated for different winds

Figures 4.6 and 4.7 show the time-series of the major bending moment above the connection, in shut-down and start-up events in the cut-out wind speed of 25 m/s and turbulence intensity of 12.83 %.

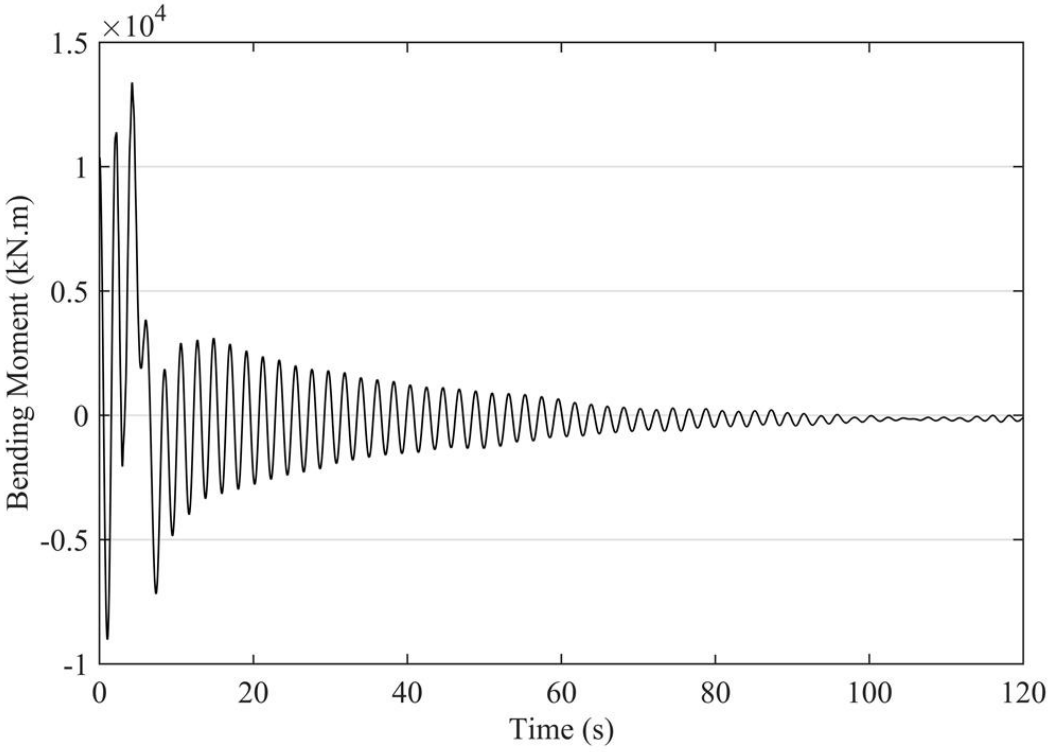

Figure 4.6. Major bending moment in the shut-down event

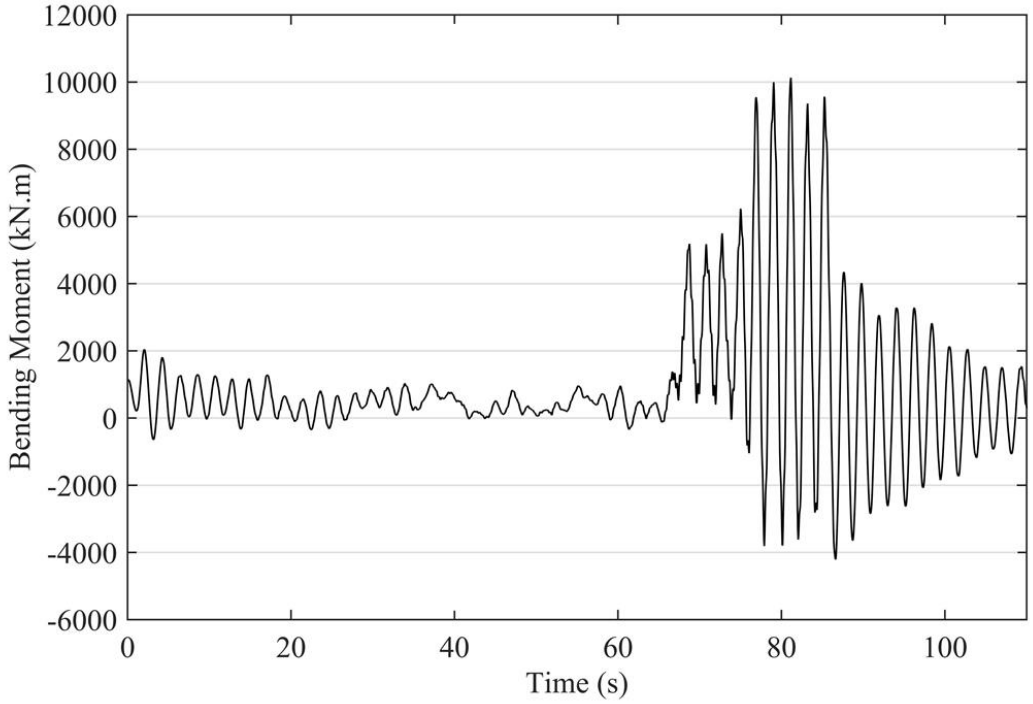

Figure 4.7. Major bending moment in the start-up event

4.2. Finite Element Modeling of the Connection Region

In this section, details of the FE model of the bolted connection are described. Subsequently, modeling results are validated using the strain gauge measurements.

4.2.1. Details of the Model

A shell type Finite Elements (FE) model of the bolted connection connecting the lower and middle parts of the tower (location of which is marked in Figure 3.2 and details of which are shown in Figures 3.3 and 3.4 is produced in ABAQUS [4] FE software. Flanges and wall of the tower connection are modeled by 3520 quadrilateral shell elements, while the 88 bolts connecting the two flanges are modeled by beam elements. Modulus of elasticity of steel is assumed to be $E = 2.1 \times 10^5$ MPa and a Poisson's ratio of $\nu = 0.3$ is assumed, according to Eurocode [45]. Figure 4.8 shows the FE model developed for the connection. A 0.304 m segment of wall below the connection level and a 0.414 m segment above it are included in the model. In order to model the interaction between the flanges, a 4 mm gap is included between the shells representing the flanges as shown in Figure 4.9, and compression-only connector elements are placed between the nodes of the two flanges. Bolt preloads are applied by assigning coefficients of thermal expansion to the materials of beam elements and applying a fictitious temperature field to them. The forces and moments calculated by the aero-dynamic analysis at the cross section above the connection and the displacements and rotations calculated at the cross section below the connection are applied as time-varying boundary conditions.

4.2.2. Analysis Results and Strain Records

Bolt stress time-series are then obtained from FE analyses. Figure 4.10 shows the stress time-series of the bolt in the 233° position, calculated for six sets of wind parameters, with the wind turbine in the operating conditions. Figures 4.11 and 4.12 show the time-series of bolt stresses in shut-down and start-up events.

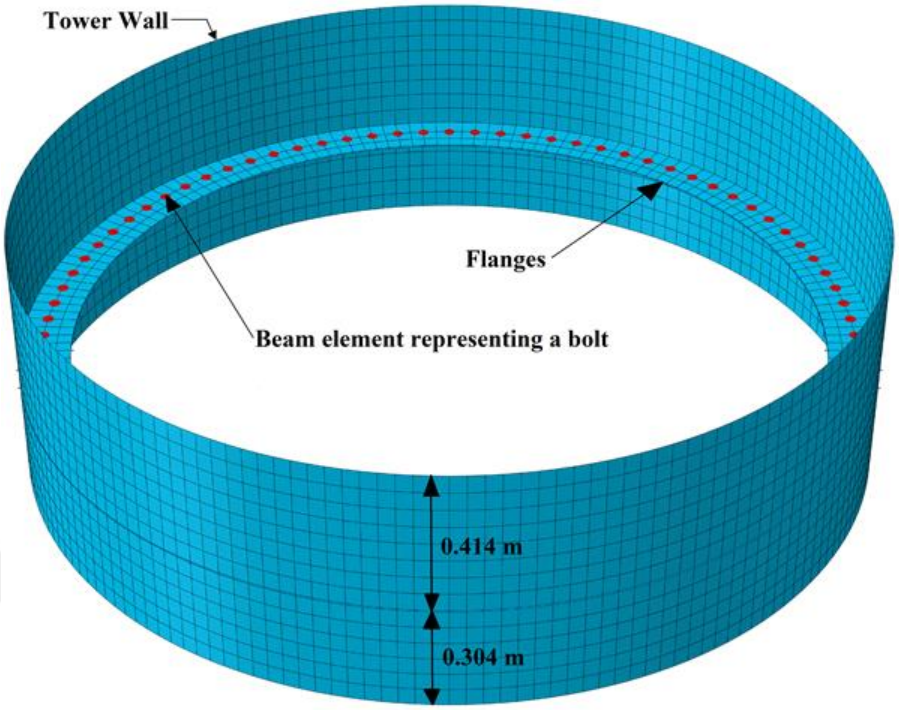

Figure 4.8. Finite element model of the connection region

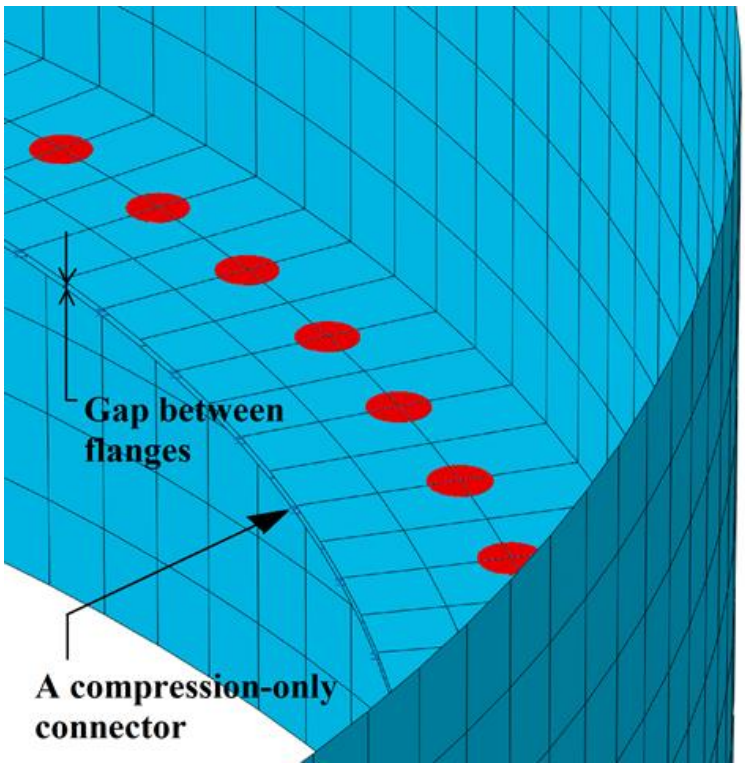

Figure 4.9. A view of the finite element model around bolts and flanges

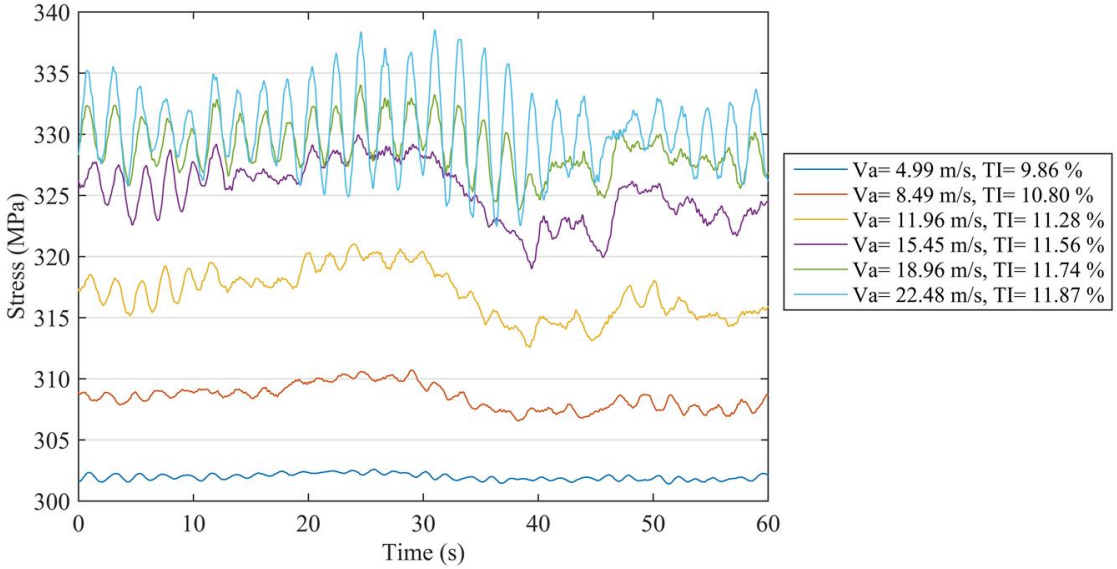

Figure 4.10. Numerically generated stress time-series for the bolt at 233^0 position

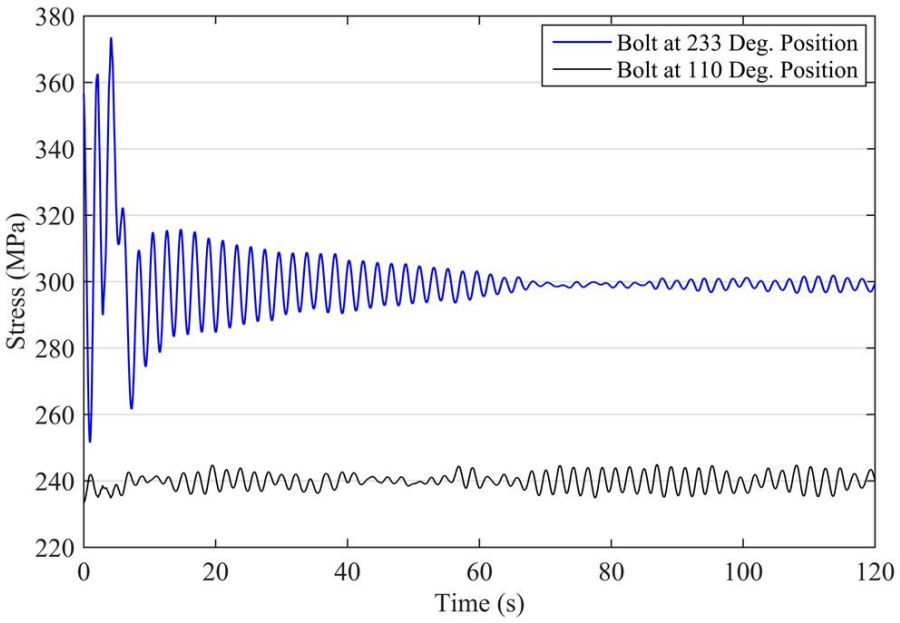

Figure 4.11. Stress time-series of two bolts in shut-down event

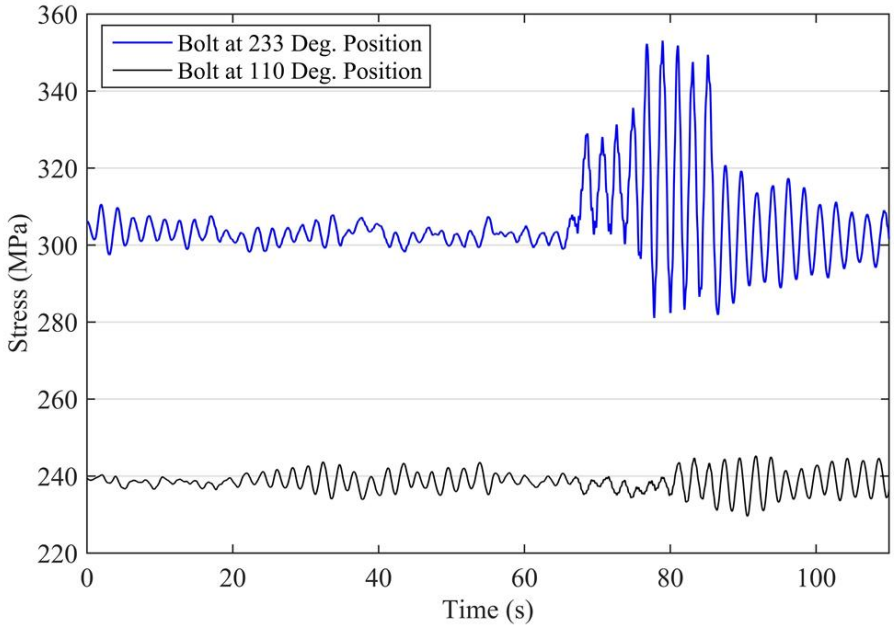

Figure 4.12. Stress time-series of two bolts in start-up event

A strain record was obtained from strain gauges inside bolts at 233° and 110° positions on 2015/04/01, at 15:42:30. Wind speed measurements from the weather station, for that specific date and time, indicate an average wind speed of 5.90 m/s and a turbulence intensity of 21.67 % for the hub height. Figures 4.13 and 4.14 show the numerically generated stress time-series for bolts at 233° and 110° positions for wind parameters $V_a = 5.90$ m/s and $TI = 21.67$ % and measurements from strain gauges inside those bolts recorded on 2015/04/01, at 15:42:30. Since fatigue damage is related to ranges of stress (or strain) cycles, the mean values are subtracted from strain records, and zero-mean stress time series are plotted.

Figures 4.15 and 4.16 show the power density spectra of the stress time-series shown in Figures 4.13 and 4.14. The plotted spectra show satisfactory agreement between the simulation and measurement results.

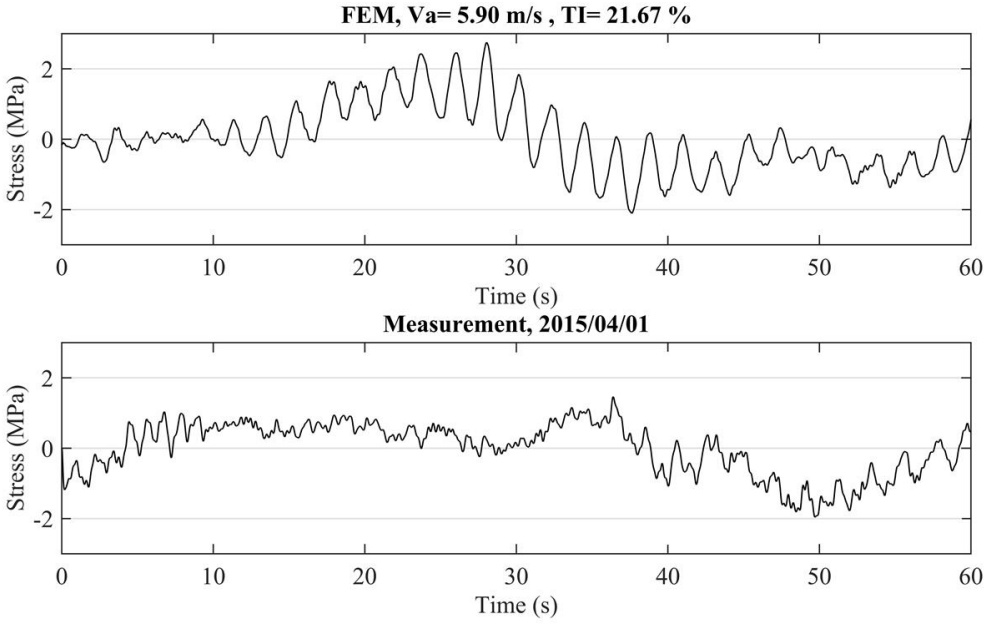

Figure 4.13. Stress time-series from simulations and measurements of the bolt at 233^0 position

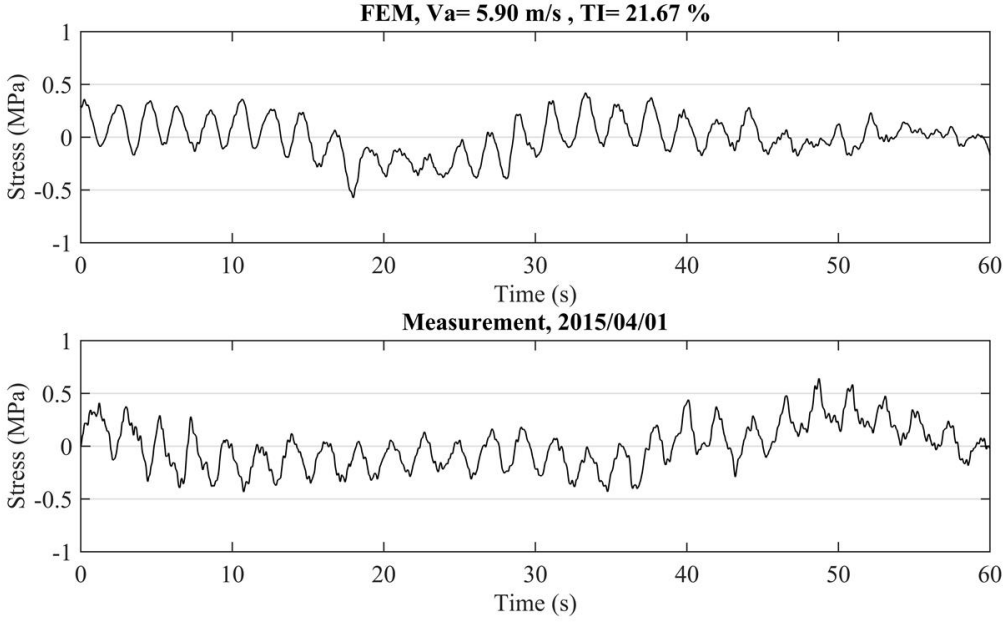

Figure 4.14. Stress time-series from simulations and measurements of the bolt at 110^0 position

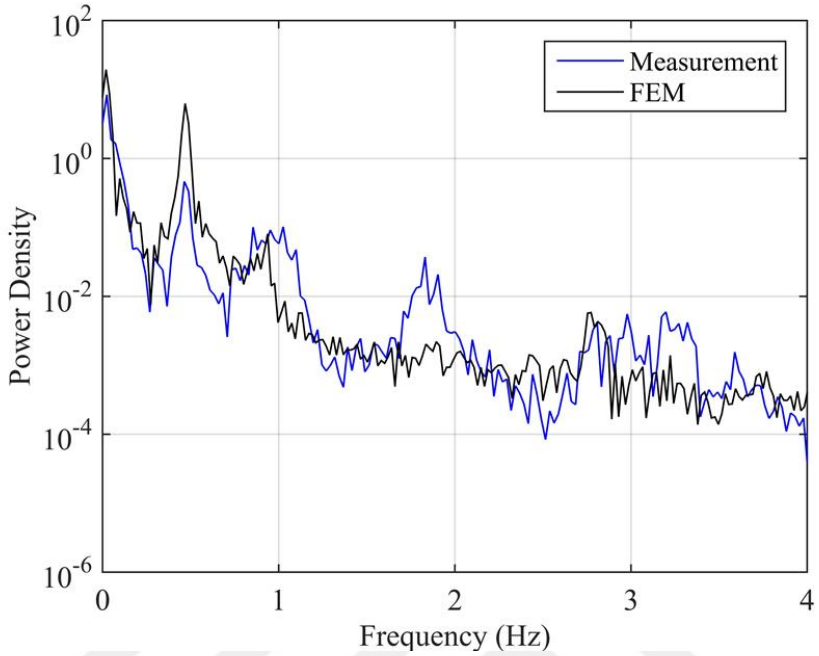

Figure 4.15. Power spectral density of stress time-series, bolt at 233^{0} position

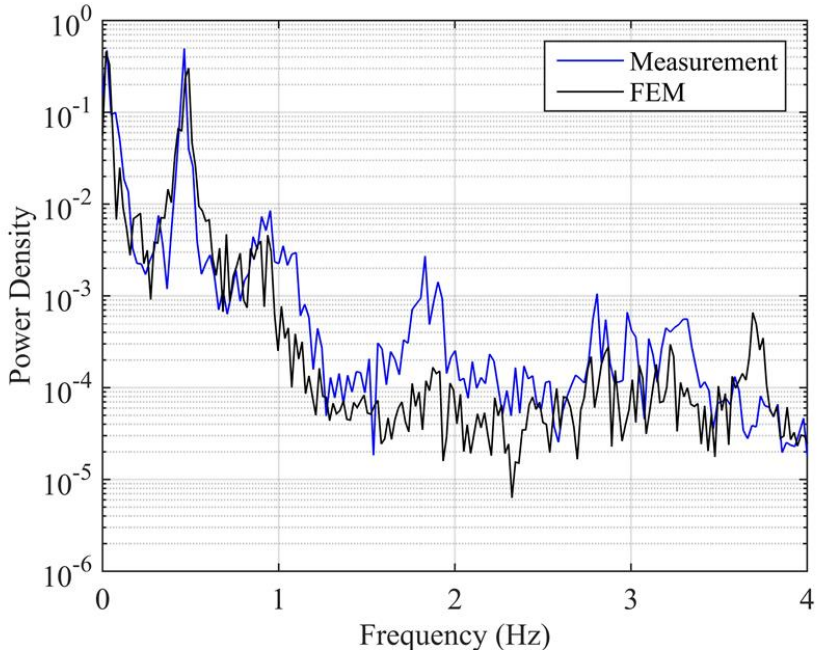

Figure 4.16. Power spectral density of stress time-series, bolt at 110^{0} position

4.3. Fatigue Damage Estimation Procedure

In order to estimate the fatigue damage caused by an arbitrary stress time-series, first it should be converted to a set of constant amplitude cyclic time-series, with different stress ranges, using a procedure named cycle-counting. Cycle counting is performed using a computer code written based on the rainflow algorithm given in ASTM [5]. This method of cycle-counting is applied to all of the stress time-series obtained for sets of wind parameters.

Figures 4.17 and 4.18 show the stress range histograms obtained by cycle counting the stress time-series shown in Figures 4.13 and 4.14.

Figure 4.19 shows the stress range histograms obtained by cycle counting the numerically generated stress time-series of the bolt at 233° position in 1 min of loading, calculated for the case of $V_a = 4.99$ m/s, and different representative values of TI. In the same way, stress range histograms are obtained for all the other sets of representative values of wind parameters. Using the probabilities shown in Figure 4.2 as weighting factors for the histograms shown in Figure 4.19, the average stress range histogram for the case of $V_a = 4.99$ m/s is calculated. Figure 4.20 shows the stress range histograms of the bolt at 233° position for all the representative values of V_a obtained by applying the same procedure. The probabilities of occurrence shown in Figure 4.1 are used as weighting factors for histograms shown in Figure 4.20, and an average stress range histogram is obtained for the bolt at 233° position. Figure 4.21 shows the average yearly stress range histograms obtained for the bolts at 233° and 110° position, caused only by operational times of the turbine. On the other hand, Figures 4.22 and 4.23 show the stress range histograms caused by a shut-down and a start-up event.

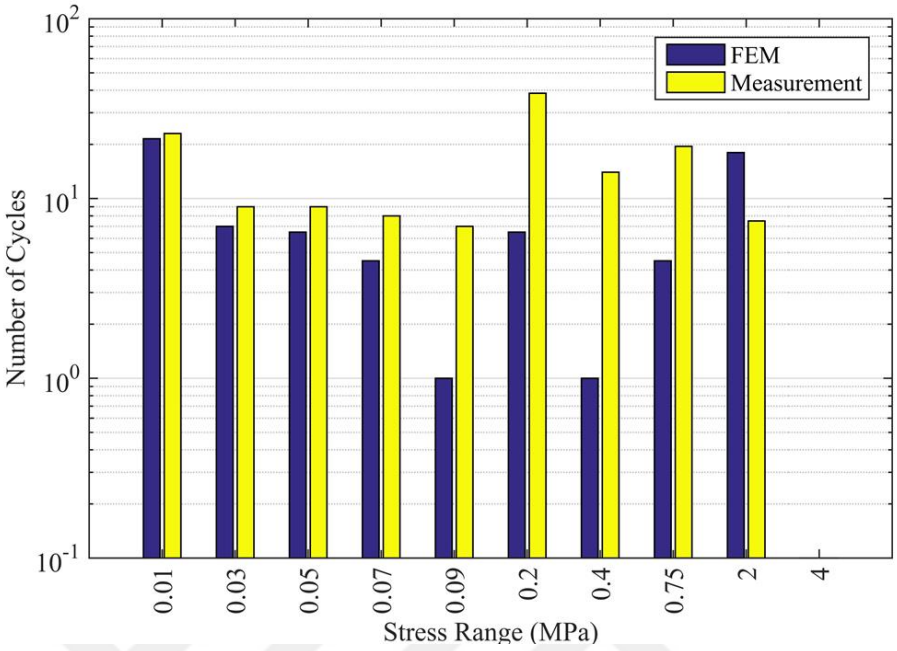

Figure 4.17. Histograms of stress ranges in the bolt at 233^0 position, simulation vs. measurement

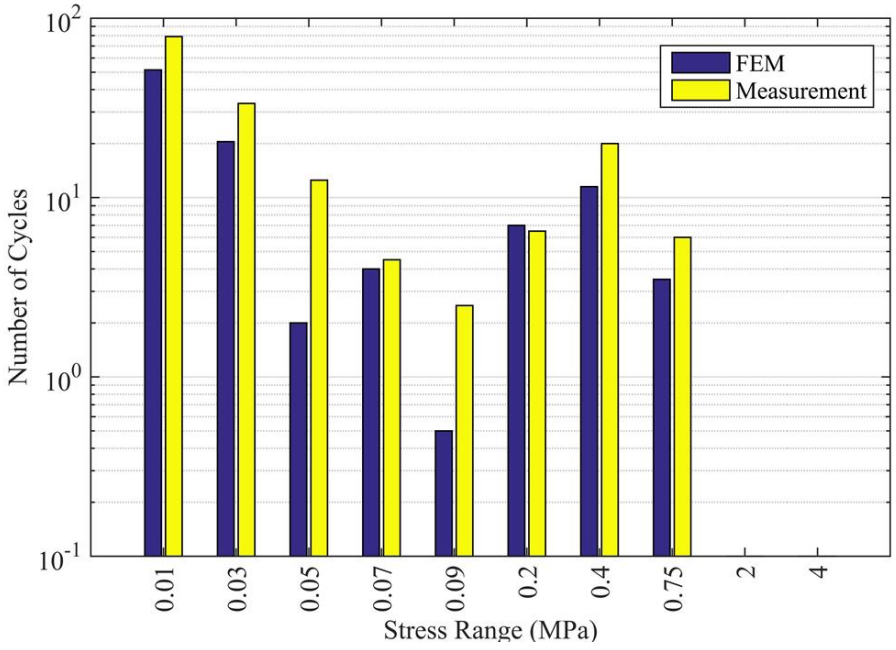

Figure 4.18. Histograms of stress ranges in the bolt at 110^0 position, simulation vs. measurement

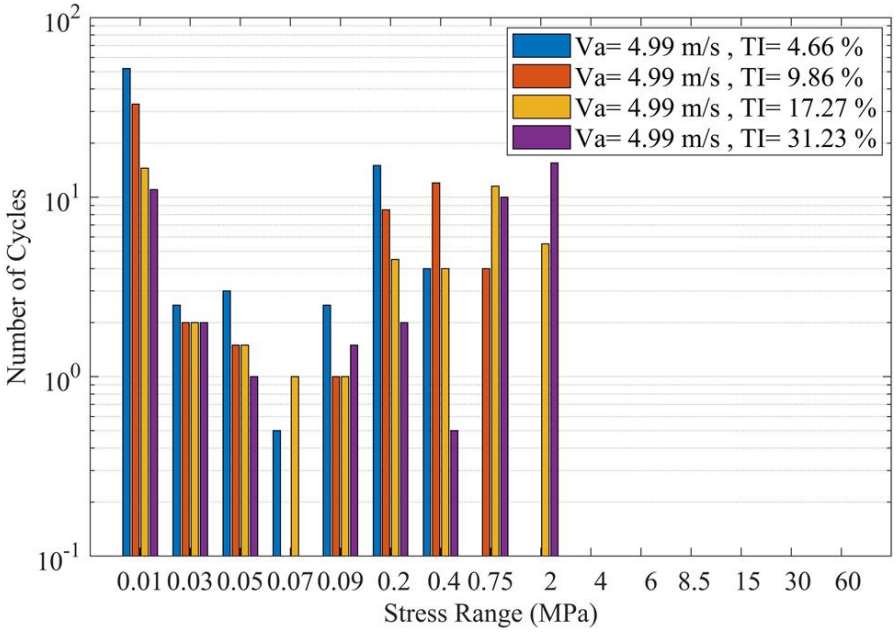

Figure 4.19. Stress range histograms for Bolt at 233^0 position, for $V_a = 4.99$ m/s and different TI values in 1 min

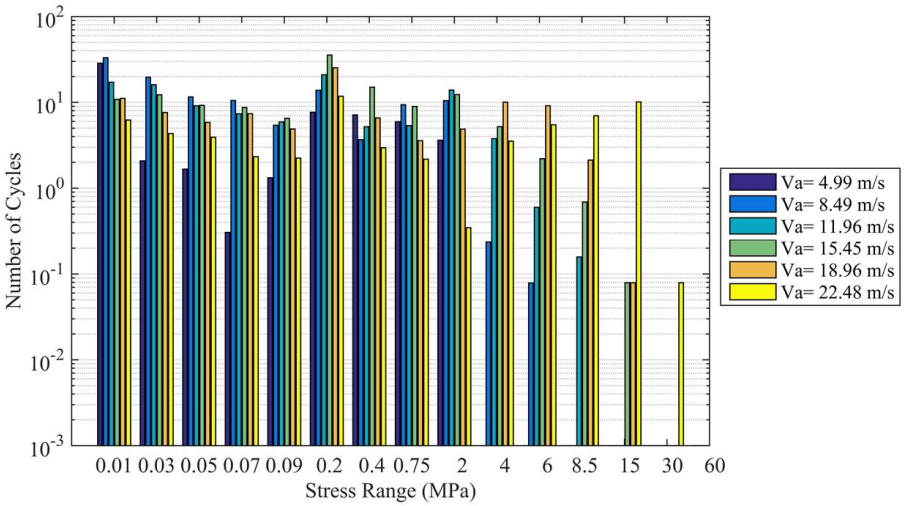

Figure 4.20. Stress range histograms for Bolt at 233^0 position, for different V_a values in 1 min

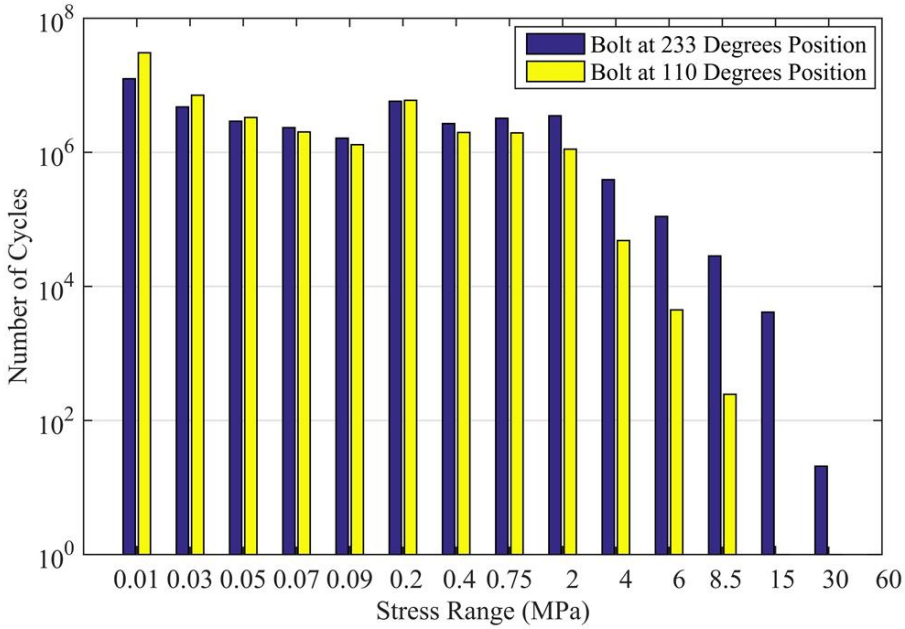

Figure 4.21. Stress range histograms for two bolts in 1 year, caused by only operational times

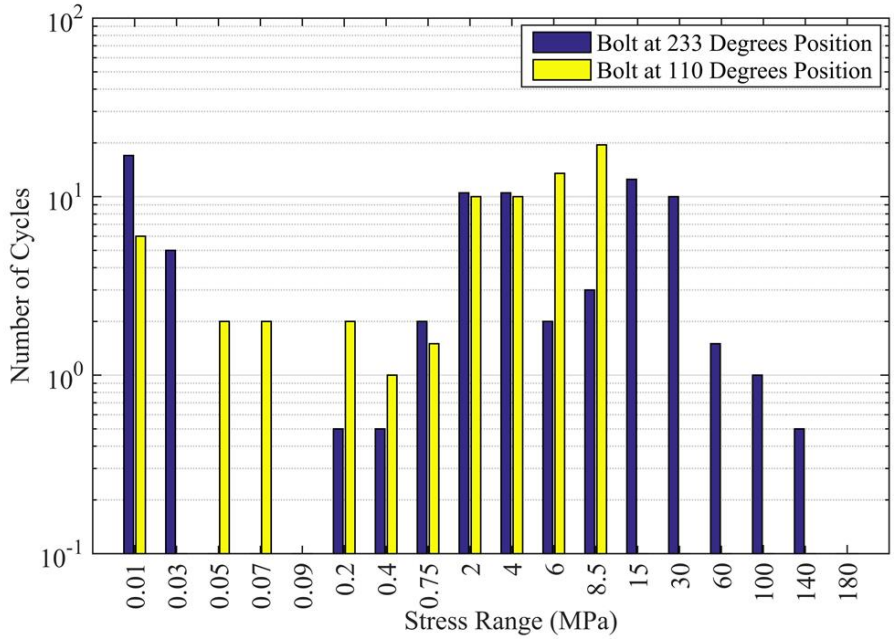

Figure 4.22. Stress range histogram caused by a shut-down event

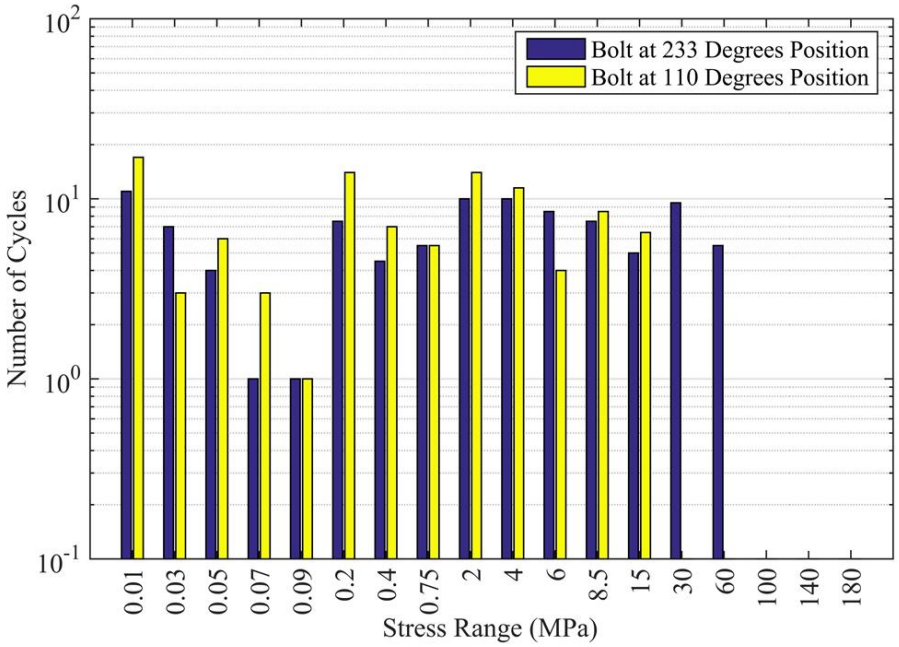

Figure 4.23. Stress range histogram caused by a start-up event

The Palmgren-Miner damage index as described in Eurocode [6] is used in this research. This index can be calculated by Eq. 4.7:

$$D = \sum_i \frac{n_i}{N_i} \tag{4.7}$$

where n_i is the number of stress cycles of a certain range, and N_i is the number of stress cycles with that range that would cause structural failure as a result of fatigue. The damage index D reaching 1.0 indicates fatigue failure. N_i values for different stress ranges (S_i) are usually provided in the form of S-N curves. The fatigue analyses of this research are based on the nominal stress method and employ the S-N curve provided by Eurocode [6] for the nominal stress method. The S-N curve that Eurocode [6] recommends for a M36 bolt represents a 95 % survival probability for Log$N$, which is a conservative S-N curve. A mean S-N curve represents a 50 % survival probability. With the assumption of normal distribution for Log$N$, the S-N curve of Eurocode [6] should be shifted as much as $1.64 \times s_{\text{Log}N}$ towards higher values, where $s_{\text{Log}N}$ is the standard deviation of Log$N$ and is set to 0.2 for lack of information, according to the instructions of DNVGL [46]. Moreover, the threshold value of fatigue strength (cut-off) is removed from the S-N curve, as suggested by DNVGL [47]. The mean S-N curve used for damage calculations is shown in Figure 4.24.

The uncertainty of the number of cycles for failure at any stress range (represented here by the probability distribution assigned to the S-N curve values) has several sources. Among these sources of uncertainty, existence of voids inside the bolt steel, random distribution of inclusions (e.g. carbon particles) inside the steel, and pre-existing cracks resulting from coating and manufacturing of the bolt threads can be mentioned. Since wind turbine towers are susceptible to fatigue because they are subjected to dynamic loads almost continuously, special attention should be given not to use bolts which have visible cracks. Also a certain level of manufacturing quality as provided by standards is needed to control the risks arising from the undetectable cracks originating from the bolt manufacturing processes.

Using the stress range histograms of each bolt shown in Figures 4.21, 4.22 and 4.23 together with the mean S-N curve of Figure 4.24, the yearly damage index accumulated in each bolt from operational times, and the damages accumulated in one shut-down and one start-up events are calculated according to Eq. 4.7, and summarized in Table 4.1.

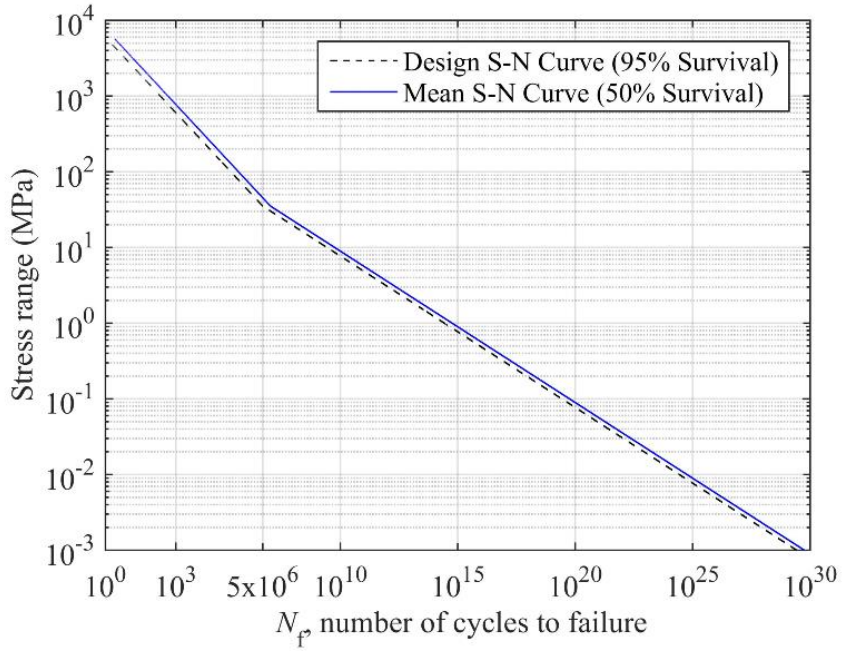

Figure 4.24. The mean S-N curve obtained for M36 bolts

Table 4.1. Damage from operational, shut-down, and start-up conditions.

Bolt Position	**Yearly Operational**	**Shut-Down**	**Start-Up**
233^0	1.090×10^{-5}	6.249×10^{-6}	2.968×10^{-6}
110^0	2.281×10^{-7}	1.704×10^{-9}	9.305×10^{-9}

Figure 4.25 shows the yearly contributions of each wind speed to the fatigue damages in the bolts. The values summarized in the chart indicate that the low probabilities of higher wind speeds compensate for the larger stress ranges.

Fatigue life of each bolt can be estimated by reciprocal of the total damage index accumulated in 1 year. Using the damage values summarized in Table 4.1, fatigue lives of the bolts can be estimated for any specific number of shut-downs and start-ups per year. Figures 4.26 and 4.27 show the estimated fatigue lives.

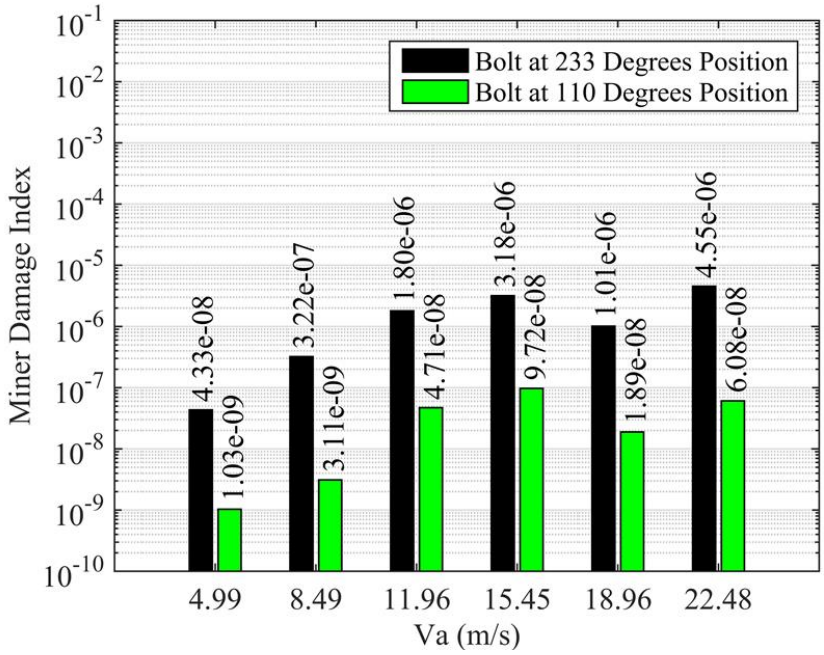

Figure 4.25. Contribution of each wind speed to the yearly damage, in the operational conditions

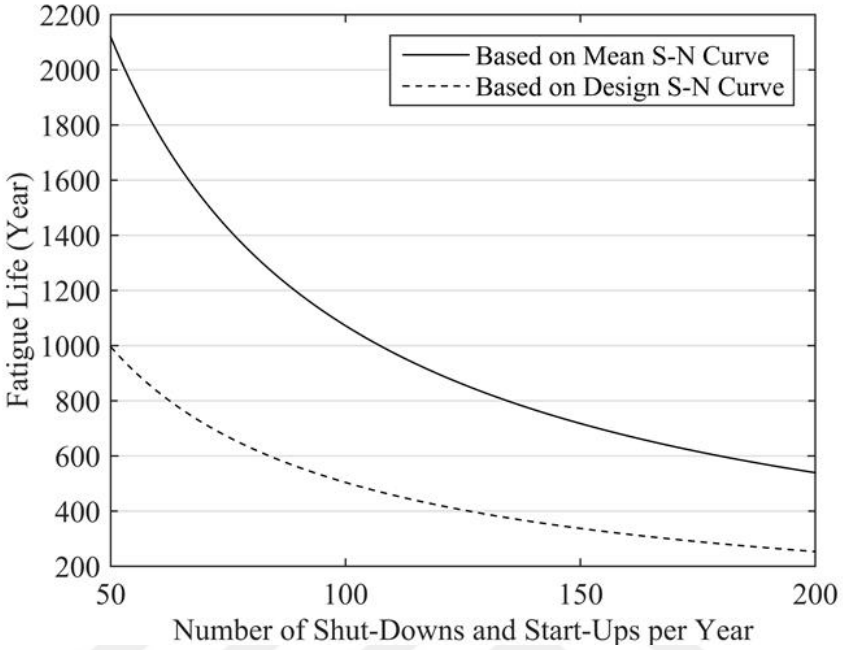

Figure 4.26. Fatigue life estimation for the bolt at 233^0 Position

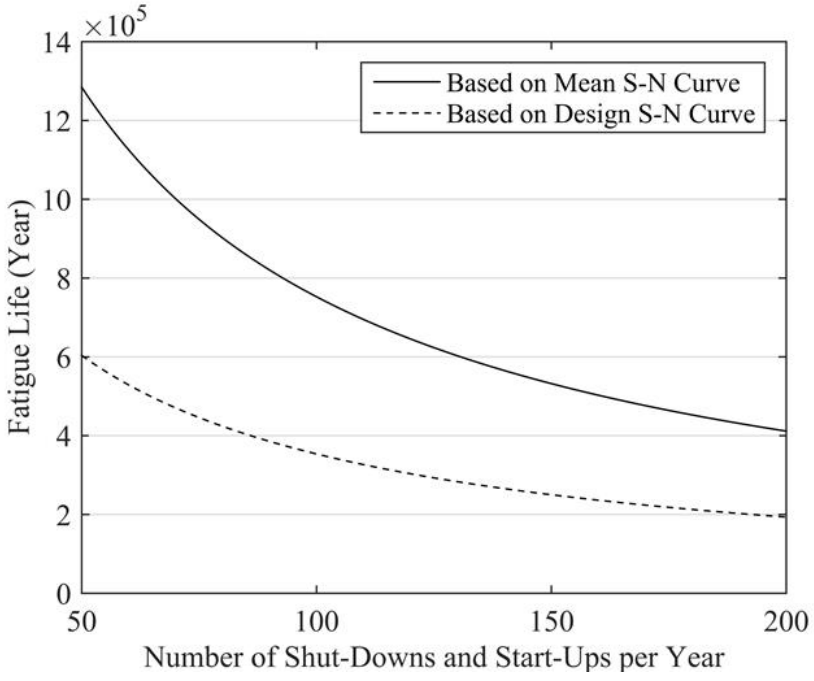

Figure 4.27. Fatigue life estimation for the bolt at 110^0 Position

4.4. Effect of Uncertainties Caused by the Random Nature of Numerically-Generated Wind Speed Time-Series

The wind field time-series produced by the TurbSim software are produced by a random number generator and depend on the numbers termed seeds, input by the operator of the software. Changing the seed number and keeping all of the other input parameters of the software unchanged, results in multiple different wind speed time-series for the same wind parameters. This may result in a change in the calculated fatigue damage depending on the chosen seed numbers. Since Miner's damage index (Eq. 4.7) is used in this research as the measure of damage, the randomness of wind time-series can only affect the calculated damage through the numbers of the counted cycles of demand on the bolt (n_i).

In order to investigate the amount of variation in the estimated damage resulting from the random nature of the generated wind time-series, for the average wind parameters of $V_a = 6.86$ m/s and $TI = 13.59$ % , 40 wind speed time-series are generated with different seed numbers. Figure 4.28 shows five of the 40 wind speed time-series at the rotor hub, generated for the same (average) values of the wind parameters. Figure 4.29 shows the major bending moment time-series above the bolted connection, for the five wind speed time-series shown in Figure 4.28. In order to estimate the variation of counted cycles (n_i) of demand on the bolts with feasible computational effort, cycle-counting is applied to the major bending moment time-series above the bolted connection. Figure 4.30 shows five of the 40 bending moment histograms obtained for randomly generated wind fields.

Taking into account all of the 40 randomly generated wind speeds, the number of cycles counted for each bin of the histogram takes 40 different values. The scattered n_i values obtained for each bin can be put into bins and presented as a histogram. The histograms of n_i obtained for the four largest bending moment bins, and the fitted lon-normal probability distributions are shown in Figures 4.31, 4.32 , 4.33 and 4.34. Here for the purpose of illustrating the procedure, the average ($\sigma_{n_{i,assumed}} = 1.98$) of

the standard deviations shown in Figures 4.31, 4.32 , 4.33 and 4.34 is assumed for the counted cycles (n_i) of in each bin of the stress range histograms obtained for 1 min loading of each wind case (eg. the histograms shown in Figure 4.19) and also for the stress range histograms of start-up and shut-down events shown in Figures 4.22 and 4.23. A comprehensive study of the probability distribution and standard deviation of the numbers of the counted cycles is recommended for future research.

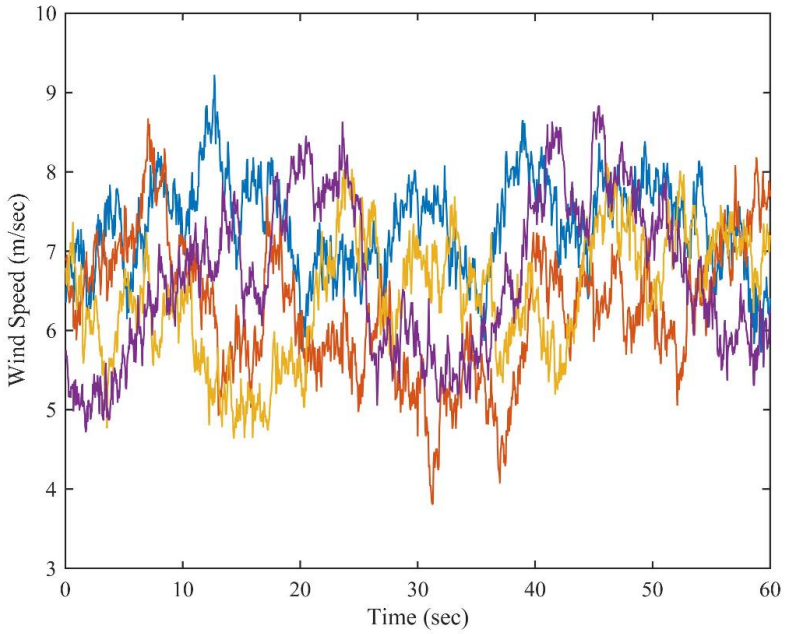

Figure 4.28. Randomly generated wind speed time series for the average values of wind parameters

In the operational conditions, the number of counted cycles in the i'th bin of the 1 min long stress range histogram corresponding to the j'th representative value of V_a (designated $n_{i,j}$) is calculated by Eq. 4.8.

$$n_{i,j} = \sum_{k=1}^{B_k} W_{j,k}.n_{i,j,k} \tag{4.8}$$

where $n_{i,j,k}$ is the number of counted cycles in the i'th bin of 1 min long stress range histogram corresponding to the j'th representative value of V_a and the k'th representative value of TI, $W_{j,k}$ is the weighting factor for the k'th representative value of TI,

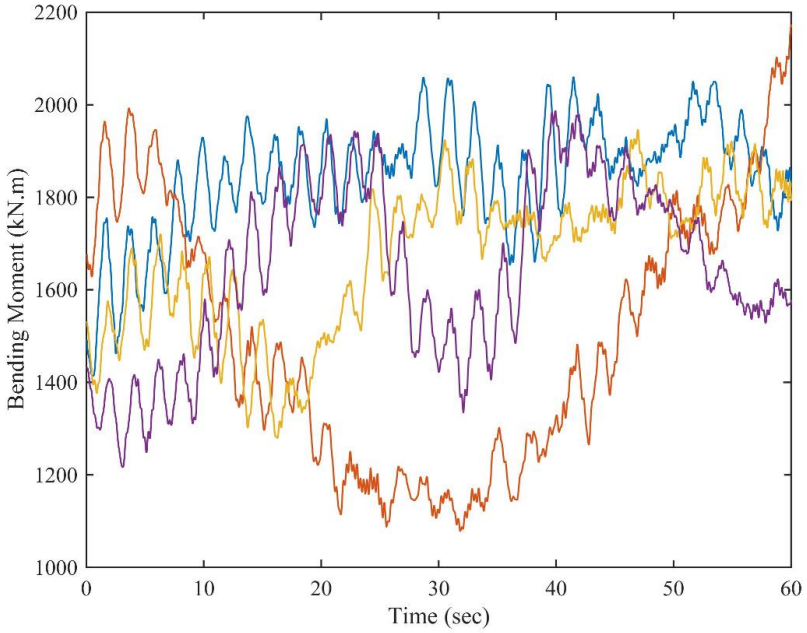

Figure 4.29. Randomly generated major bending moment time series for the average values of wind parameters

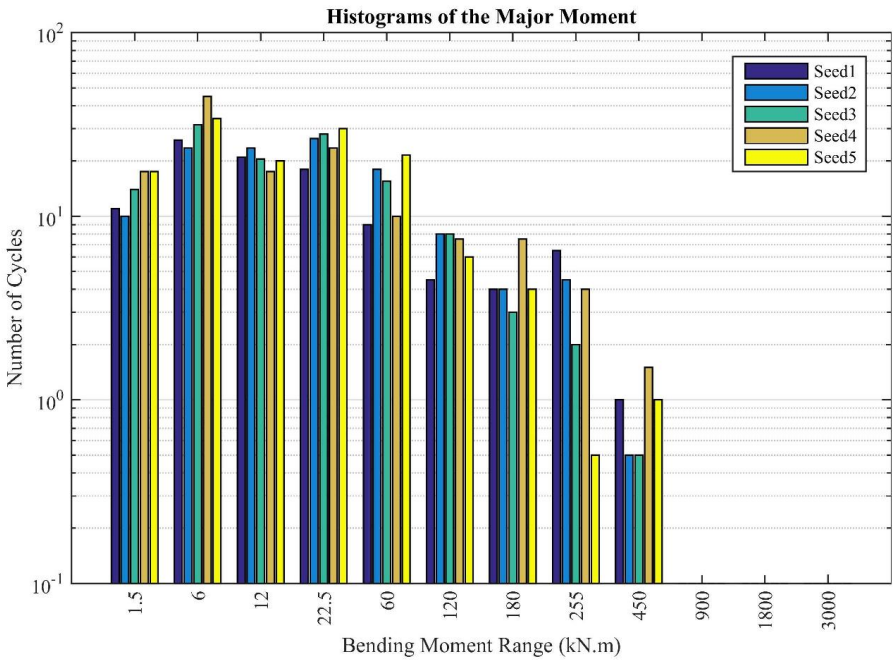

Figure 4.30. Histograms of randomly generated bending moment ranges

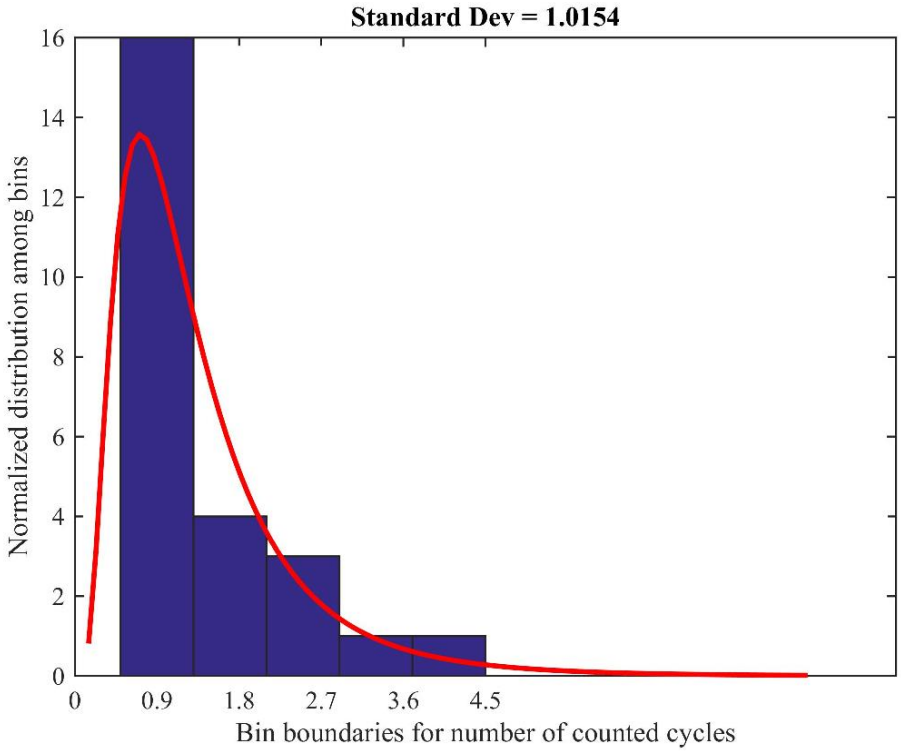

Figure 4.31. Distribution of counted cycles in the 450kN.m bin

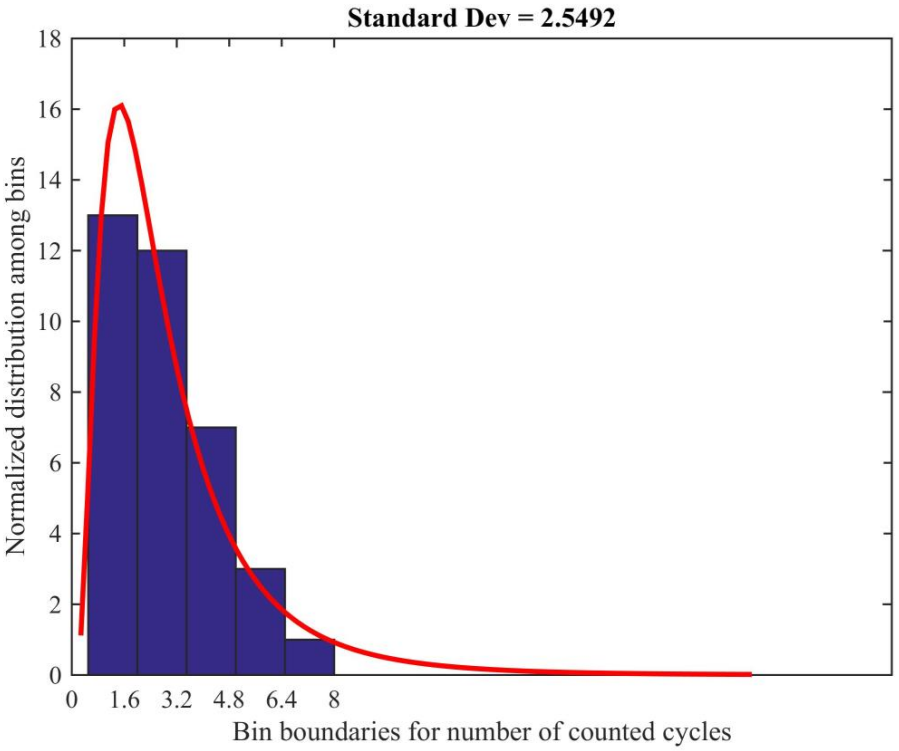

Figure 4.32. Distribution of counted cycles in the 255kN.m bin

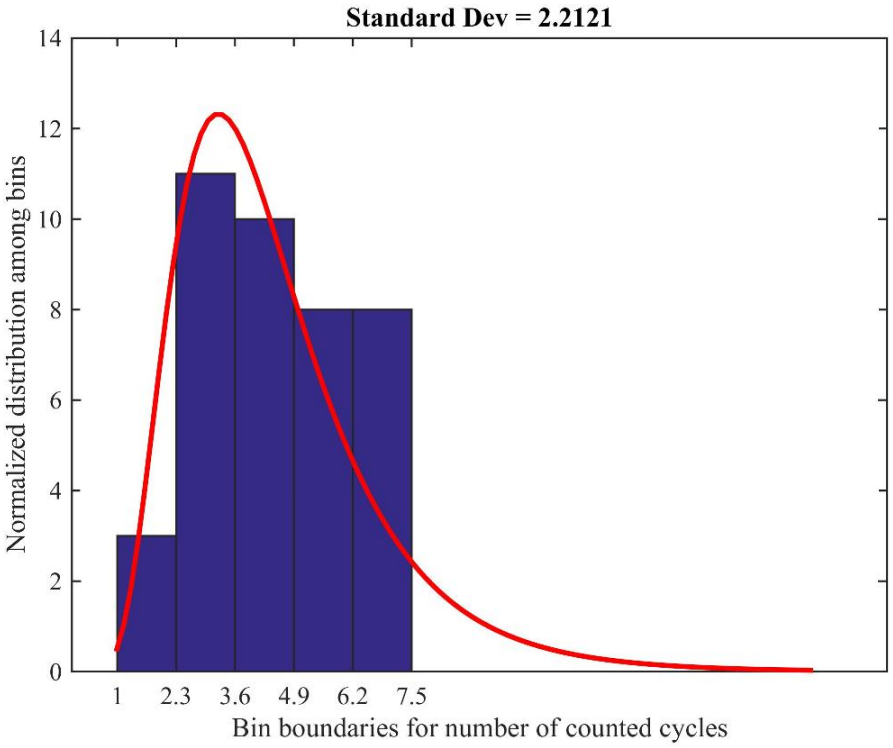

Figure 4.33. Distribution of counted cycles in the 180kN.m bin

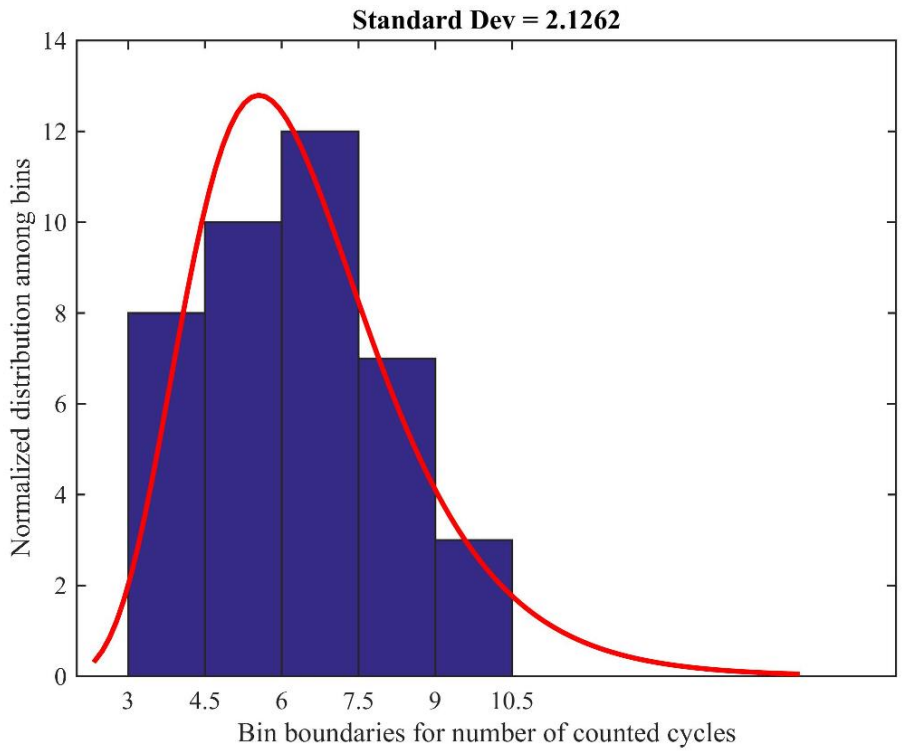

Figure 4.34. Distribution of counted cycles in the 120kN.m bin

and B_k is the number of the representative values of TI.

Since the uncertainty of the counted cycles originates from randomly generated numbers, the numbers of the counted cycles of each wind case as random variables are independent of the numbers of the counted cycles for other wind cases, and therefore are uncorrelated. Using a rule described by Nowak and Collins [48] for standard deviation of a linear combination of uncorrelated random variables, the standard deviation of $n_{i,j}$ of Eq. 4.8 can be calculated by Eq. 4.9.

$$\sigma_{n_{i,j}} = \sqrt{\sum_{k=1}^{B_k} W_{j,k}^2 . \sigma_{n_{i,j,k}}^2} \tag{4.9}$$

The number of counted cycles in the i'th bin of one year long operational stress range histogram (designated $n_{i,operational}$) is calculated by Eq. 4.10.

$$n_{i,operational} = (\text{number of minutes in a year}). \sum_{j=1}^{B_j} W_j . n_{i,j} \tag{4.10}$$

where B_j is the number of the representative values of V_a, and W_j is the weighting factor for the j'th representative value of V_a. Therefore, similar to the Eq. 4.9, standard deviation of $n_{i,operational}$ in Eq. 4.10 can be obtained by Eq. 4.11.

$$\sigma_{n_{i,operational}} = (\text{number of minutes in a year}). \sqrt{\sum_{j=1}^{B_j} W_j^2 . \sigma_{n_{i,j}}^2} \tag{4.11}$$

Substituting the $\sigma_{n_{i,assumed}} = 1.98$ value (explained earlier in this section) for the $\sigma_{i,j,k}$ in Eq. 4.9 and then using the Eq. 4.11, the standard deviation of the counted cycles in each bin of the yearly operational stress range histogram is estimated to be $\sigma_{n_{i,operational}} = 2.975 \times 10^5$.

For the start-up and shut-down events, the number of cycles in the i'th bins of the yearly start-up and shut-down stress range histograms (designated $n_{i_{start-up,yearly}}$

and $n_{i_{shut-down,yearly}}$ respectively) can be calculated by Eqs. 4.12 and 4.13.

$$n_{i_{start-up,yearly}} = N_{start-up}.n_{i_{single\ start-up}} \tag{4.12}$$

$$n_{i_{shut-down,yearly}} = N_{shut-down}.n_{i_{single\ shut-down}} \tag{4.13}$$

where $n_{i_{single\ start-up}}$ and $n_{i_{single\ shut-down}}$ are the numbers of counted cycles in the i'th bins of the start-up and shut-down stress range histograms shown in Figures 4.23 and 4.22 respectively, while $N_{start-up}$ and $N_{shut-down}$ are the yearly numbers of start-up and shut-down events. For any known numbers of $N_{start-up}$ and $N_{shut-down}$, the standard deviations of $n_{i_{start-up,yearly}}$ and $n_{i_{shut-down,yearly}}$ (designated $\sigma_{n_{i_{start-up,yearly}}}$ and $\sigma_{n_{i_{shut-down,yearly}}}$) can be calculated by Eqs. 4.14 and 4.15.

$$\sigma_{n_{i_{start-up,yearly}}} = N_{start-up}.\sigma_{n_{i_{single\ start-up}}} \tag{4.14}$$

$$\sigma_{n_{i_{shut-down,yearly}}} = N_{shut-down}.\sigma_{n_{i_{single\ shut-down}}} \tag{4.15}$$

For the purpose of illustrating the procedure, assuming $N_{start-up} = N_{shut-down} = 100$ and substituting the $\sigma_{n_{i,assumed}} = 1.98$ value (explained earlier in this section) for the $\sigma_{n_{i_{single\ start-up}}}$ and $\sigma_{n_{i_{single\ shut-down}}}$ in Eqs. 4.14 and 4.15, the values $\sigma_{n_{i_{start-up,yearly}}} = 198$ and $\sigma_{n_{i_{shut-down,yearly}}} = 198$ are obtained.

On the other hand, as explained in the previous section, a normal distribution for Log$N$ with a standard deviation of $s_{\mathrm{Log}N} = 0.2$ is assumed according to instructions of DNVGL [46]. Assuming a normal distribution for Log$N$ means a log-normal distribution for N. It should be noted that the term Log$N$ designates the base 10 logarithm of N. Therefore, the standard deviation of the natural logarithm of N_i term in Eq. 4.7 is $s_{\mathrm{Ln}N_i} = s_{\mathrm{Log}N_i}/\mathrm{Log}2.71828 = 0.4605$.

According to Nowak and Collins [48], for a log-normally distributed random variable X, the relationships between the mean and standard deviation of the variable (μ_X and σ_X) and standard deviation and mean of natural logarithm of the variable ($\sigma_{\mathrm{Ln}(X)}$ and $\mu_{\mathrm{Ln}(X)}$) are given by Eqs. 4.16 and 4.17.

$$\sigma^2_{\mathrm{Ln}(X)} = \mathrm{Ln}\left(\frac{\sigma^2_X}{\mu^2_X} + 1\right) \tag{4.16}$$

$$\mu_{\mathrm{Ln}(X)} = \mathrm{Ln}\left(\mu_X\right) - \frac{1}{2}\sigma^2_{\mathrm{Ln(X)}} \tag{4.17}$$

Miner's damage index (Eq. 4.7) can be rewritten as Eq. 4.18, where d_i as defined in Eq. 4.19 is the quotient of two log-normally distributed random variables, and therefore is log-normally distributed itself, according to Nowak and Collins [48]. Furthermore, mean and standard deviation of natural logarithm of d_i can be obtained according to Eqs. 4.20 and 4.21 [48].

$$D = \sum_i d_i \tag{4.18}$$

$$d_i = \frac{n_i}{N_i} \tag{4.19}$$

$$\mu_{\mathrm{Ln}(d_i)} = \mu_{\mathrm{Ln}(n_i)} - \mu_{\mathrm{Ln}(N_i)} \tag{4.20}$$

$$\sigma_{\mathrm{Ln}(d_i)} = \sqrt{\sigma^2_{\mathrm{Ln}(n_i)} + s^2_{\mathrm{Ln}(N_i)}} \tag{4.21}$$

The value $s_{\mathrm{Ln}(N_i)} = 0.4605$ (explained earlier in this section) is put into Eq. 4.21. $\sigma^2_{\mathrm{Ln}(n_i)}$ is calculated according to Eq. 4.22, where to μ_{n_i} the counted cycles are assigned, separately from the operational, start-up and shut-down yearly histograms, and for σ_{n_i},

the values $\sigma_{n_{i,operational}}$, $\sigma_{n_{i_{start-up,yearly}}}$ and $\sigma_{n_{i_{shut-down,yearly}}}$ are assigned depending on the event for which the damage is being calculated. On the other hand, $\mu_{\mathrm{Ln}(n_i)}$ in Eq. 4.20 is calculated using Eq. 4.23. Moreover, $\mu_{\mathrm{Ln}(N_i)}$ in Eq. 4.20 is calculated by Eq. 4.24, where for μ_{N_i} the values from the mean S-N curve are entered.

$$\sigma^2_{\mathrm{Ln}(n_i)} = \mathrm{Ln}\left(1 + \frac{\sigma^2_{n_i}}{\mu^2_{n_i}}\right) \tag{4.22}$$

$$\mu_{\mathrm{Ln}(n_i)} = \mathrm{Ln}\left(\mu_{n_i}\right) - \frac{1}{2}\sigma^2_{\mathrm{Ln}(n_i)} \tag{4.23}$$

$$\mu_{\mathrm{Ln}(N_i)} = \mathrm{Ln}\left(\mu_{N_i}\right) - \frac{1}{2}s^2_{\mathrm{Ln}(N_i)} \tag{4.24}$$

A computer code is developed, which generates 200000 sets of random values for the d_i variables in Eq. 4.18 that have log-normal distributions with the parameters calculated according to Eqs. 4.20 and 4.21. Afterwards, the summation in Eq. 4.18 is performed on all of the operational, start-up and shut-down bins. Therefore, 200000 values for the yearly damage index are obtained for each bolt. Subsequently, 200000 values for fatigue lives of each bolt are obtained by calculating the reciprocals of the yearly damage index values. The calculated fatigue lives are put into 100 bins, and are shown as histograms with fitted Weibull probability distribution functions in Figures 4.35 and 4.36. The Weibull probability distribution [49] used here for fatigue lives has the probability density function given by Eq. 4.25.

$$f_W(L) = \left(\frac{\beta}{\alpha}\right)\left(\frac{L}{\alpha}\right)^{\beta-1} \mathrm{e}^{-(\frac{L}{\alpha})^{\beta}} \tag{4.25}$$

where L is the fatigue life as a random variable. The probability of failure of any bolt before L years of its life can be calculated using the Weibull Cumulative Distribution Function (CDF) given in Eq. 4.26. For the specific case of yearly 100 start-up and shut-down events and other assumptions made in this chapter, the α and β values

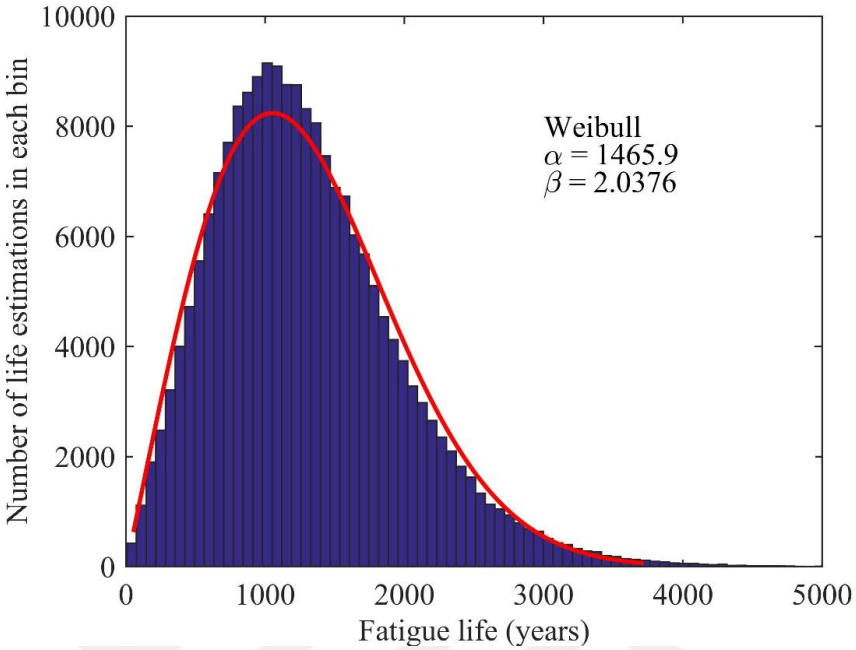

Figure 4.35. Fatigue live estimations of the bolt at 233° and the fitted Weibull distribution

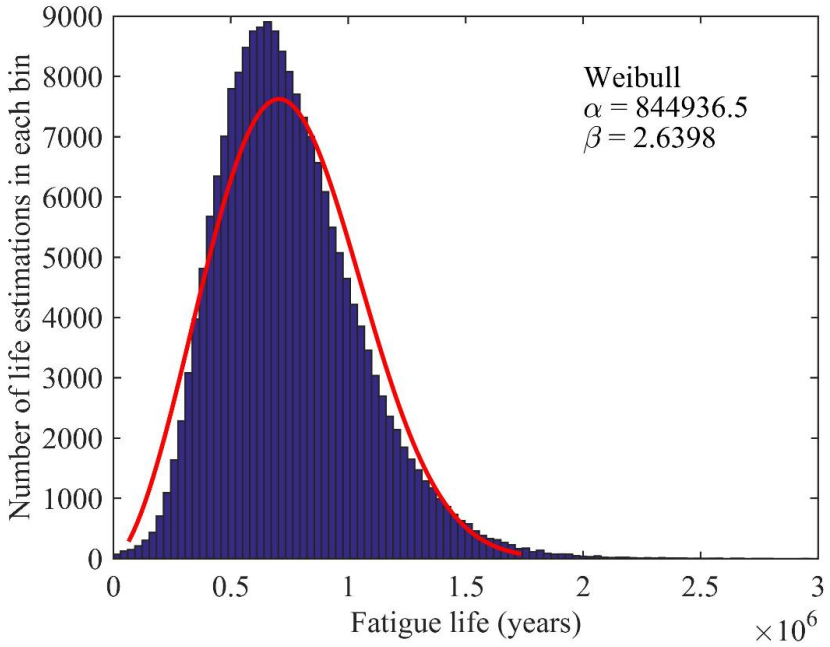

Figure 4.36. Fatigue live estimations of the bolt at 110° and the fitted Weibull distribution

shown in Figures 4.35 and 4.36 are used, and the results are shown in Figures 4.37 and 4.38.

$$F_W(L) = 1 - \mathrm{e}^{-(\frac{L}{\alpha})^{\beta}} \tag{4.26}$$

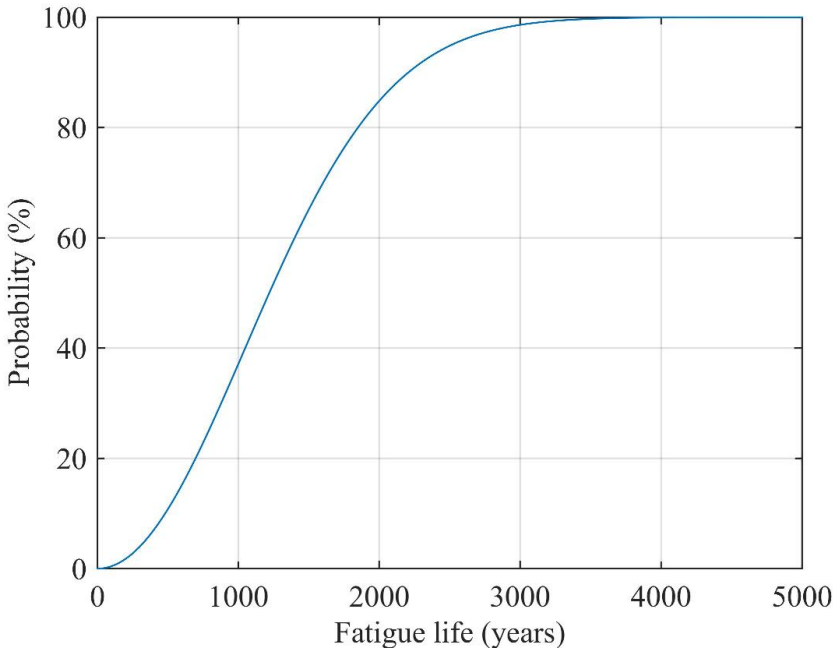

Figure 4.37. Cumulative distribution function of fatigue life of the bolt at 233°

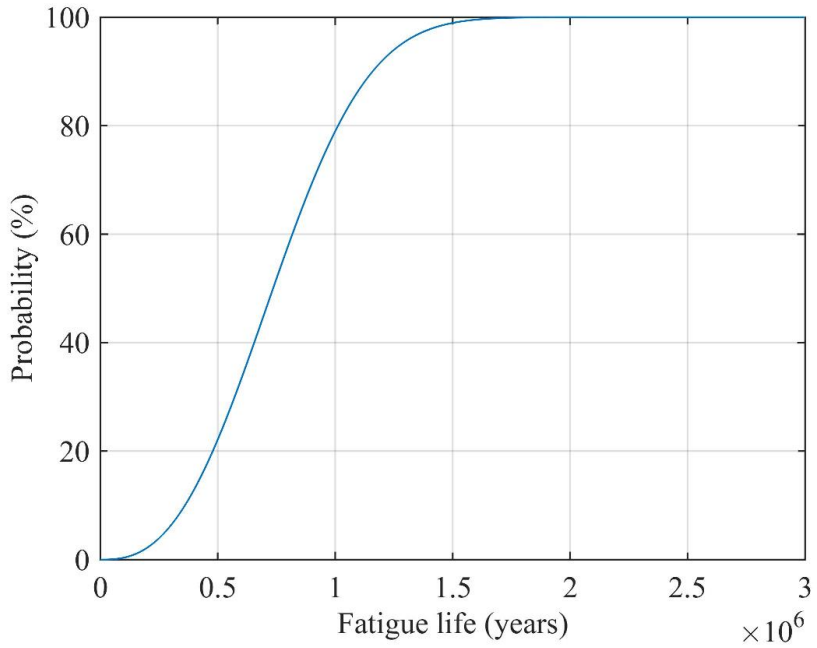

Figure 4.38. Cumulative distribution function of fatigue life of the bolt at 110°

5. LACK OF PRELOAD AND ITS EFFECT ON FATIGUE DEMANDS OF THE BOLTS

In this chapter, the effects of lack of preload on fatigue damage in the connection bolts is evaluated. The results of this chapter are also available in Badrkhani Ajaei and Soyoz [50].

5.1. Introduction to the Bolt Preload Mechanism

Fatigue damage in bolts depends on the amount of the changes of the external loads that is carried by the bolts. Therefore, in fatigue design of bolted connections, reducing the changes of bolt loads is intended [34]. Bolt preload is a tensile force produced in a bolt by application of a torque to one end of the bolt.

The bolt preloads created by the torque method differ from the design values, primarily as a result of two factors [51]: Firstly, the relationships between the torque and the preload are not exact. Secondly, due to elastic interactions of the parts of the connection, the preload in a tightened bolt decreases when another bolt near it is tightened. Consequently, an error of roughly ± 30 % must be expected in calculation of the preloads produced by torque [51]. Nagata *et al.* [52] measured the variations of the bolt preloads in a flange connection tightened by the torque method. The test results of [52] show that the preload deficiency in the bolts reach values up to 45.2 % of the intended values.

Chen *et al.* [53] investigated the variations of the nut factors (K_{nut}) of bolts, defined by Eq. 5.1.

$$T_{bolt} = K_{nut} F_{bolt} D_{bolt} \tag{5.1}$$

In Eq. 5.1, T_{bolt} is the tightening torque, F_{bolt} is the bolt preload, and D_{bolt} is the diameter of the bolt. The findings of [53] indicate that for large bolts, non-lubricated bolts have higher nut factors reaching in some cases nearly twice the nut factor of lubricated bolts.

Liu *et al.* [54] investigated the self-loosening of bolts subjected to cyclic loading. The test results of [54] showed that loss of preload depends on the initial preload, and the amplitude of the cyclic loads. The test results include a case of preload loss of nearly 40 %.

Empirical relationships are available for the portion of the external loads that is transferred to the bolt in a bolted connection. For the case of a bolted joint which is loaded along the symmetry line, Pedersen and Pedersen [35,36] represented the bolted joints by two stiffness terms, where the changes of the external load (ΔP_{ex}) that is transferred to the bolt (ΔP_b) is calculated using the ratio of the two stiffness terms, according to Eq. 5.2:

$$\Delta P_b = \frac{k_b}{k_b + k_m} \Delta P_{ex} \tag{5.2}$$

where k_b and k_m are the stiffness terms representing the bolt and the connected members respectively. For an axi-symmetric joint with one bolt, Williams *et al.* [34] conducted experiments and FE analyses. Relationships based on the stiffness coefficients in Eq. 5.2 were proven to be inaccurate, while FE analysis results were more accurate.

Hobbs *et al.* [55] indicated that fatigue damage in the bolted joints depends on several factors including the stiffnesses of the connected members, stiffness of the bolt, and the amount of preload. Therefore, the results of that study cannot be generalized to larger bolts which are used in wind turbine towers with significantly thicker flanges.

Since the numerical methods are more economical and flexible than the experimental approaches and field measurements, numerical methods have an essential role in design, evaluation and research. However, behavior of the bolted connections are complicated. According to [56], distribution of contact stresses between flanges produces secondary forces in the bolts. Huang *et al.* [57] indicate that the flexibility of the flange affects the bolt loads. Analysis of bolted flange connections used in wind turbine towers is difficult because of large dimensions, large number of the bolts, and the interactions between the connected members and the bolts. Consequently, simplifications are needed in order to reduce the computational efforts. Schaumann and Eichstädt [30] explains a common method of design for bolted ring flange connections, where a segment of the connection which includes only one bolt, and is subjected to the maximum load is isolated and is used for the calculations.

Many studies on the subject of bolt preloads (e.g. [34–36]) do not address the nature of the areodynamic loads which are characteristic of wind turbine towers. Moreover, the research on wind turbine towers (e.g. [27, 28, 31]) does not consider the effect of preloads on bolt fatigue, in a detailed and quantitative way.

This chapter presents a numerical evaluation of effects of bolt preload on fatigue damage in the maximally loaded bolt of a bolted connection subjected to aerodynamic loads of a wind turbine. The research presented in this thesis does not determine the safety or quality of products of any specific designer or manufacturer.

5.2. Aero-Dynamic Simulation for the Bolt Preload Study

The yearly average of wind speed which was assumed for design of this wind turbine (10 m/s) is assigned to the average of the wind speed time-series (V_a) for producing the wind field in this chapter. The case study turbine is a class $\mathrm{I_A}$ turbine according to the [24] categorization. Consequently, the reference turbulence intensity is assumed to be $I_{ref} = 0.16$. According to [24], for any value of V_a the mean σ_V can be obtained by by Eq. 4.3.

For $V_a = 10$ m/s, μ_{σ_V} is estimated to be 1.808 m/s, using Eq. 4.3, and this mean value is assigned to σ_V, and a turbulence intensity of $TI = 18.08$ % is calculated using Eq. 4.1. Figure 5.1 displays the down-wind component of wind speed at hub of the rotor, produced by the TurbSim software.

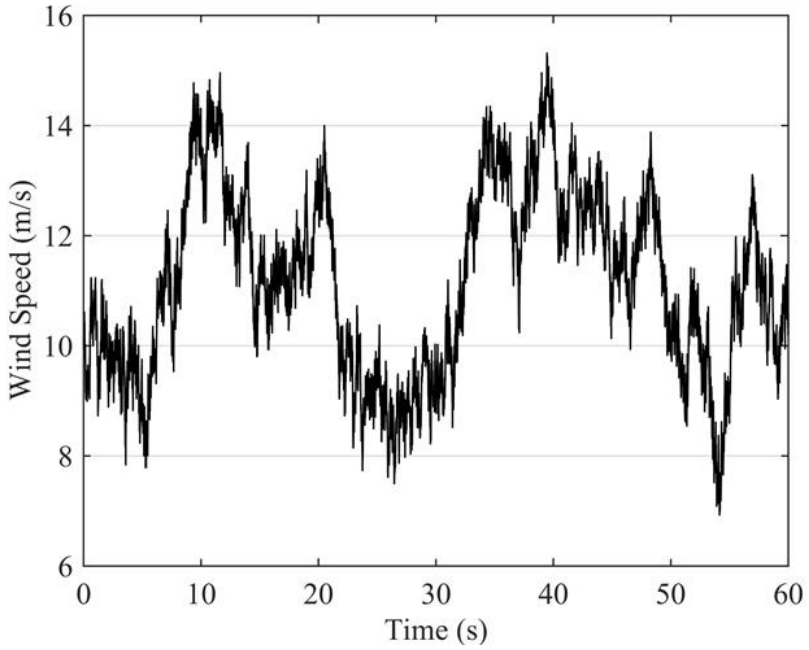

Figure 5.1. Time-series of wind speed at hub center of the rotor plane, in the downwind direction

The FAST [3] software is used to simulate the aerodynamic loads. The time-series of the bending moment and axial force, in a cross-section of the tower 414 mm above the connection connecting the lower and middle parts, marked in Figure 3.2 is shown in Figures 5.2 and 5.3.

5.3. Finite Element Modeling of the Connection Segment

Similar to the method used by [30], a segment of the bolted connection which includes one bolt, and is the maximally loaded segment is modeled in this chapter. The modeled segment is positioned at the frontmost side of the connection from an upwind viewing angle. Using the vertical symmetry plane of the bolt, only half of this

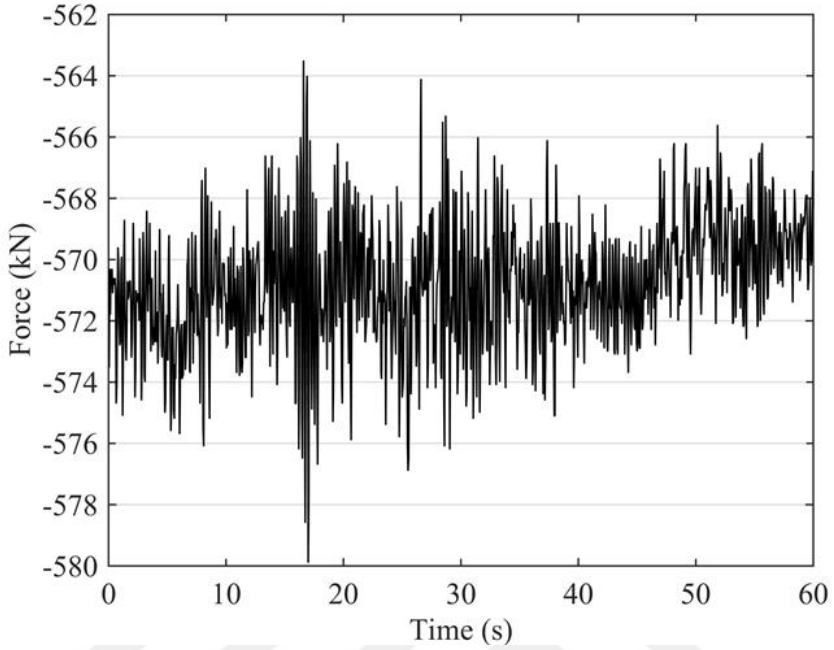

Figure 5.2. Axial force above the bolted connection

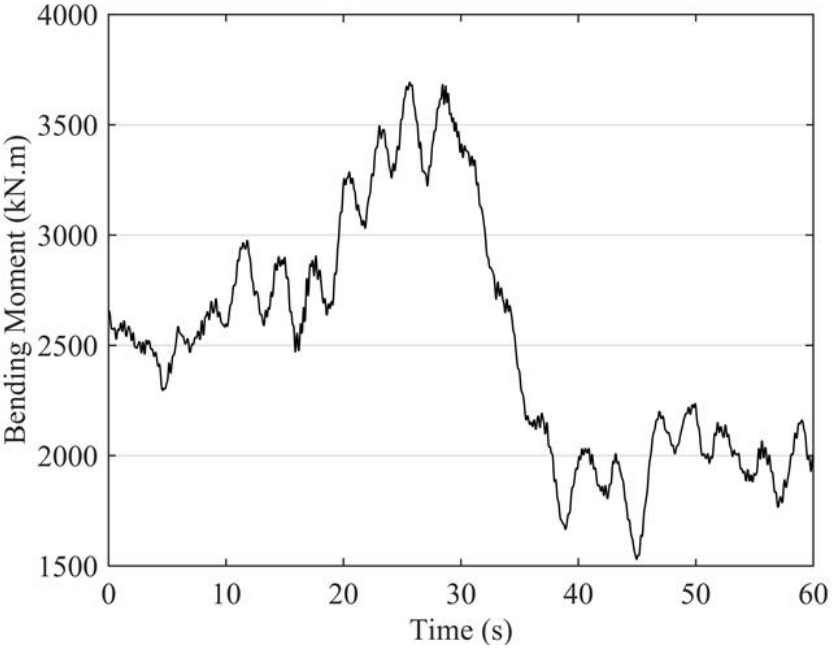

Figure 5.3. Bending moment above the connection

segment is modeled in the ABAQUS [4] FE software. The FE mesh of the segment is shown in Figure 5.4. Modulus of elasticity of steel is assigned the value $E = 210$ GPa, based on [45]. The FE model has 70300 linear wedge elements. Symmetry boundary conditions are assigned to the symmetry plane. Tie constraints are assigned to the interfaces between the washers, the bolt head, the nut, and the bolt shank. Contact is assigned to the interface of the flanges, and the coefficient of friction is assumed to be $\mu = 0.45$, as recommended for surface categories A and B in [58]. Contacts are assigned to the interfaces between the washers and the flanges, where a coefficient of friction of $\mu = 0.25$ is assumed, according to the recommendations of [59] for galvanized steel surfaces.

As it was explained earlier in Section 5.1, as a result of several factors which include the inaccuracy of the relationship between the torque and preload, the interactions of the connection members, faulty construction, and loosening of the bolts, the preloads in the bolts show a significant variation. In order to investigate the effects of preload deficiency on bolt fatigue, the preload values in Table 5.1 are assigned to the bolt in the model. As shown in Table 5.1, the preload assigned to the bolt is decreased step by step, in order to calculate the effect of preload over a wide range, starting from the design preload and ending at a value near zero (10^{-6} kN).

Table 5.1. Preloads assigned to the bolt in the FE model

Bolt Preload (kN)	**Applied Preload / Design Preload**
510	100 %
255	50 %
127.5	25 %
51	10 %
10^{-6}	0 %

The lower edge of the wall in the model is assigned fixed boundary conditions and the vertical traction t_V calculated using Eq. 5.3 is assigned to the upper edge of

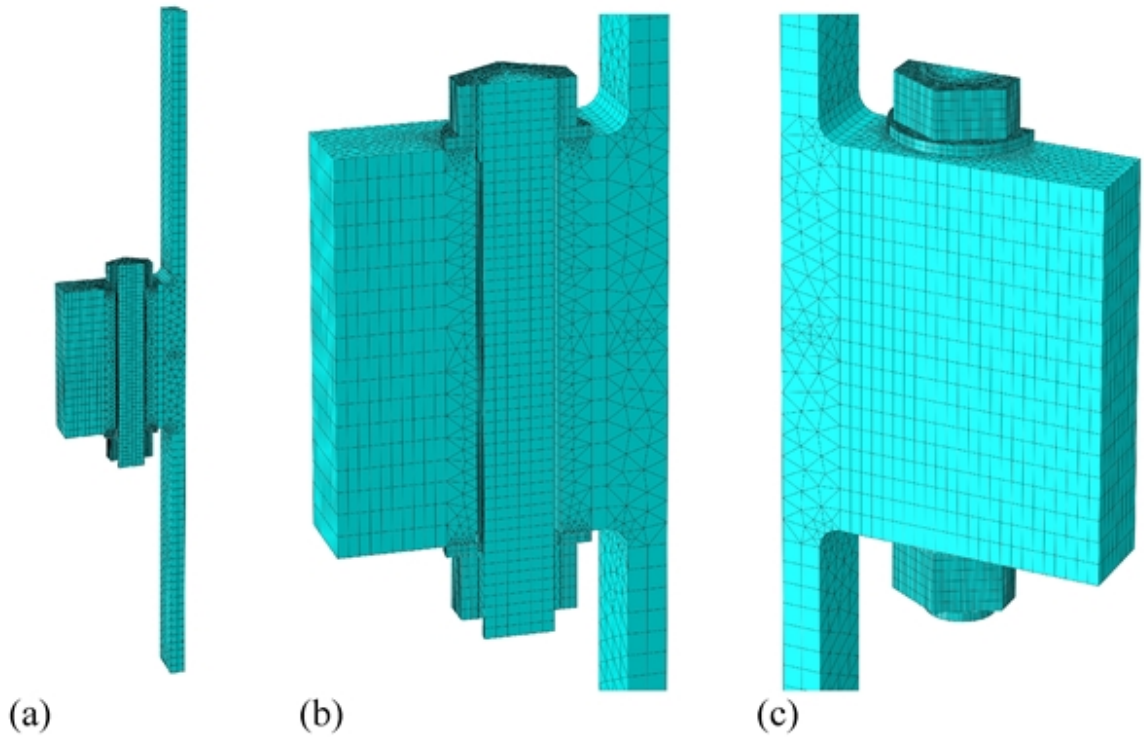

Figure 5.4. The finite element model: (a) Side view, (b) The connection region from the side of the symmetry plane, (c) The connection region from outside

the wall.

$$t_V = \frac{F_{Axial}}{A_{Tower}} + \frac{M_{Bending}}{S_{Tower}} \tag{5.3}$$

where, F_{Axial} designates the axial force in a cross section of the tower 0.414 m above the bolted connection (marked in Figure 3.2), and is shown in Figure 5.2, $M_{Bending}$ designates the bending moment, and is shown in Figure 5.3, while A_{Tower} and S_{Tower} are the cross-sectional area and elastic section modulus. The vertical traction in the upper edge of the wall is illustrated in Figure 5.5.

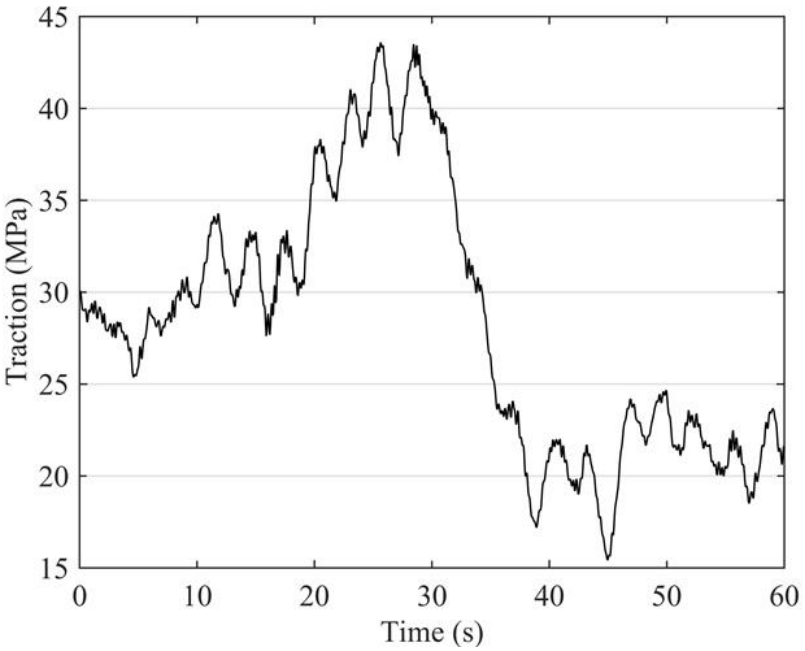

Figure 5.5. Vertical traction applied to top of the wall segment in the finite element model

5.4. Finite Element Analysis Results

In this section, the results of the FE calculations for evaluation of the effects of preload deficiency on stress ranges in the bolt are summarized. The preloads given in Table 5.1 were applied to the bolt in the FE model, and subsequently the vertical traction illustrated in Figure 5.5 was assigned to the upper edge of the wall. FE

simulations were conducted to investigate the effects of the loads on the bolt.

The normal stress contour in the direction of the symmetry axis of the bolt, under the effect of 510 kN bolt preload is shown in Figure 5.6. Based on the results

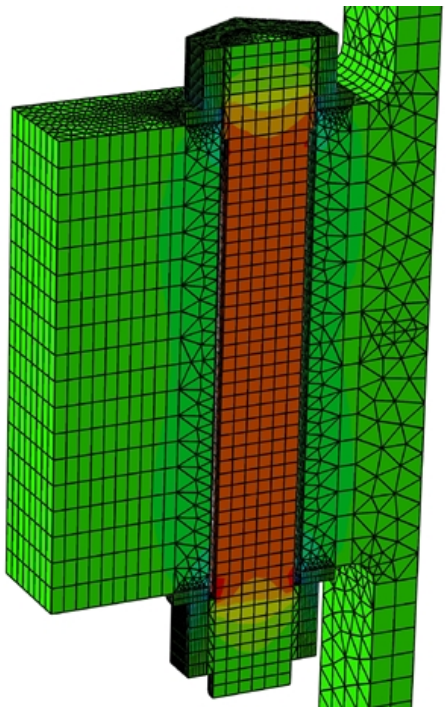

Figure 5.6. Contour of stress in the direction of bolt axis, after applying the bolt preload

of FE analyses, axial force and bending moment in the middle of the bolt length are calculated and multiplied by two (since only half of the bolted joint was modeled using symmetry). Axial forces in the bolt for the cases of multiple preload values are shown in Figure 5.7. Figure 5.8 shows the same time-series after removing their averages. Furthermore, the bending moment time-series and the same plots after removing their averages are shown in Figures 5.9 and 5.10 respectively.

The results illustrated in Figures 5.8 and 5.10, show that as the bolt preload decreases from the design value of 510 kN to a near-zero value, the ranges of cycles in the axial force and bending moment increase. The bolt stress calculated based on axial bolt force and the total bolt stress (bending stresses included) are compared in

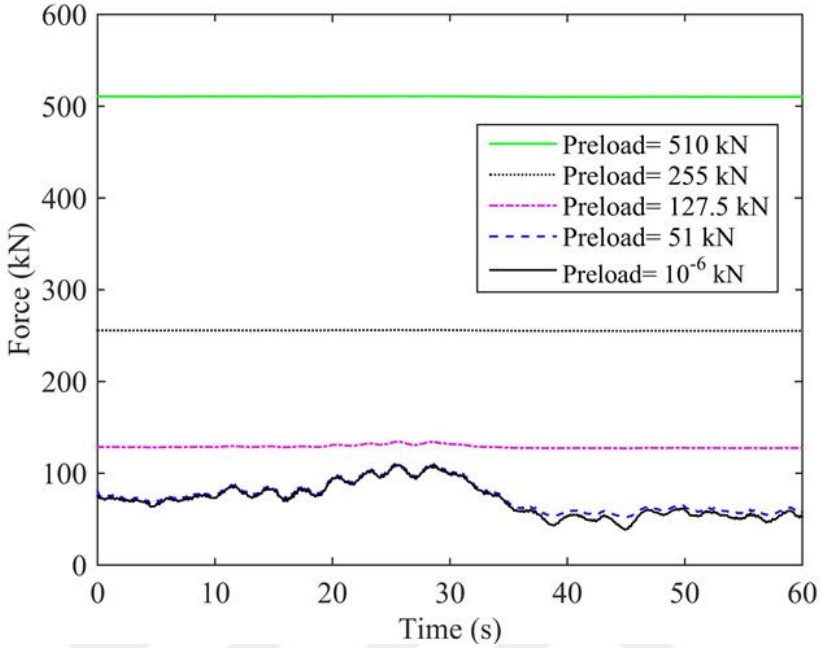

Figure 5.7. Time-series of axial force in the bolt obtained for different preload levels

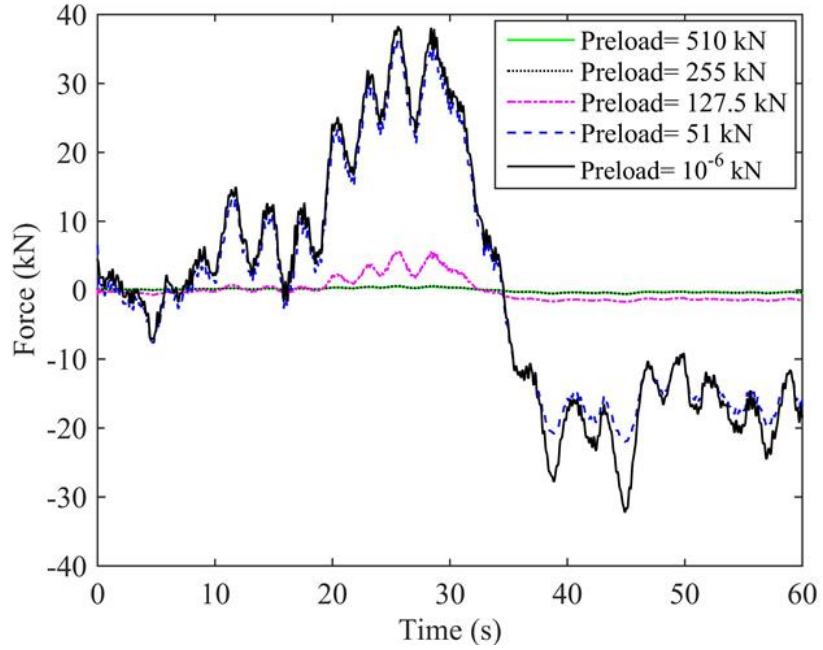

Figure 5.8. Time-series of axial force in the bolt, obtained for different preload levels, averages removed

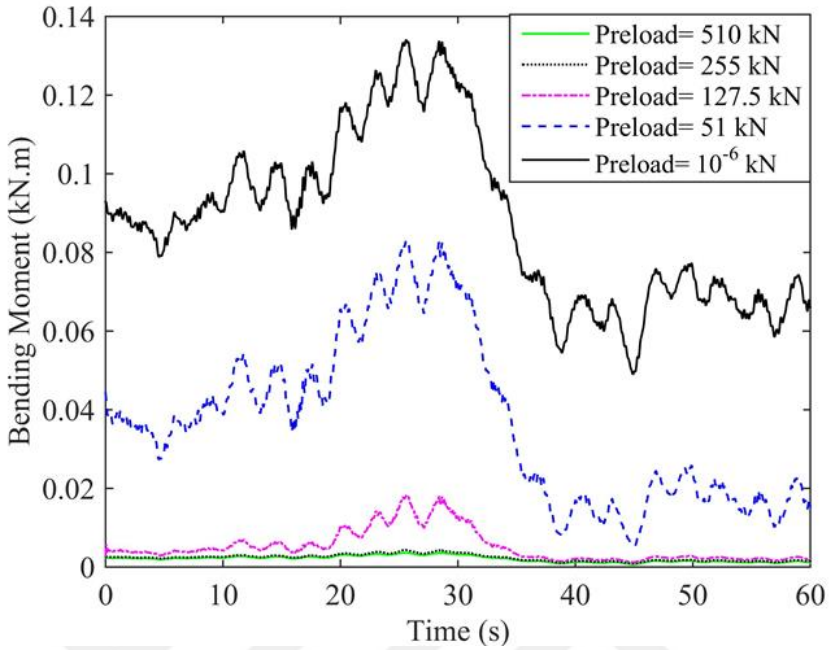

Figure 5.9. Time-series of bending moment in the bolt obtained for different preload levels

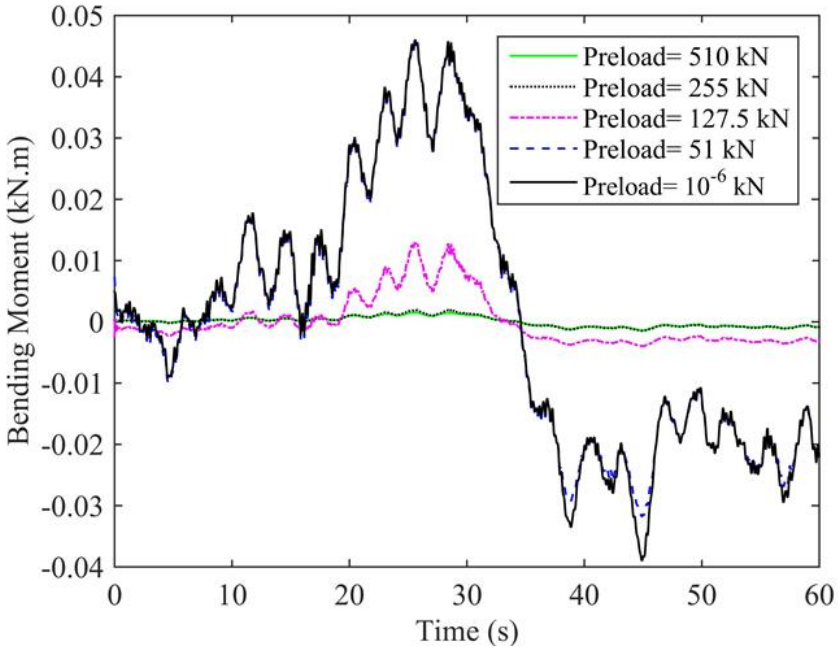

Figure 5.10. Time-series of bending moment in the bolt, obtained for different preload levels, averages removed

Figure 5.11. The same stress time-series are plotted in Figure 5.12 with their averages removed. The plots of Figure 5.12 show that including the bending stresses in the calculations results in a significant increase of the ranges of the stress cycles.

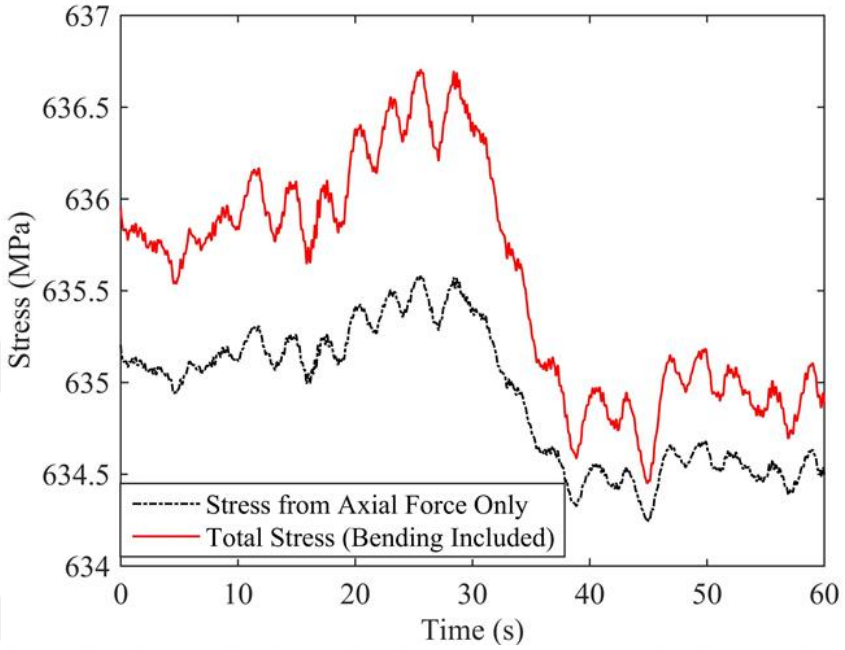

Figure 5.11. Time-series of bolt stress from axial force only, compared to the total bolt stress

Total bolt stress plots for multiple preload values are shown in Figure 5.13. The same plots with their averages removed are shown in Figure 5.14. It can be observed that reduction of bolt preload from the design value of 510 kN to a near-zero value increases the ranges of the stress cycles significantly. While change of preload from 100 % to 50 % does not result in a significant change in the ranges of bolt stress cycles, reduction of preload to 25 % causes a considerable increase in the ranges of stress.

5.5. Fatigue Analysis and Results

In order to execute the cycle-counting procedure on bolt stress according to the rainflow cycle-counting algorithm of [5], a computer code was written, and was used for cycle-counting of the stress plots in Figure 5.11. For the case of 510 kN preload,

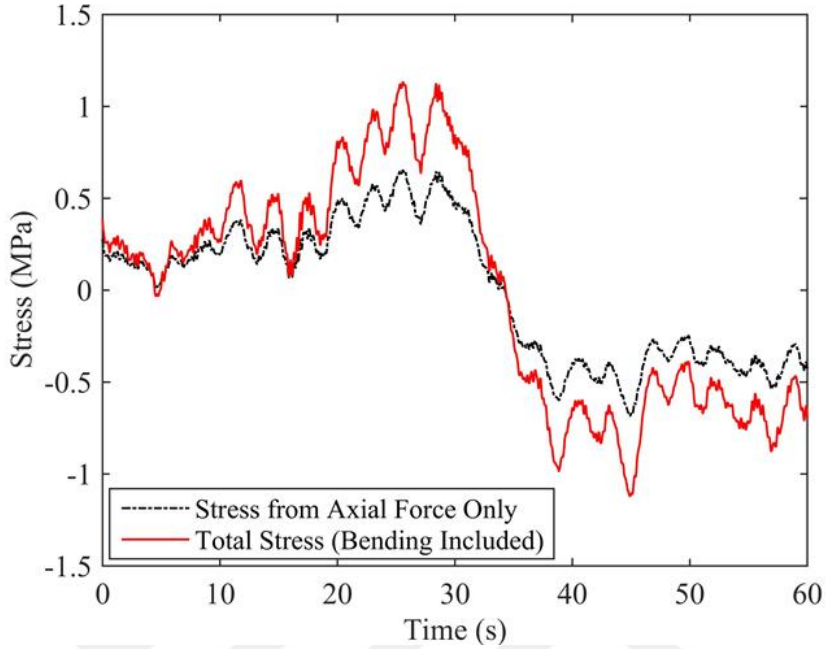

Figure 5.12. Time-series of bolt stress, from axial force only vs. total stress, averages removed

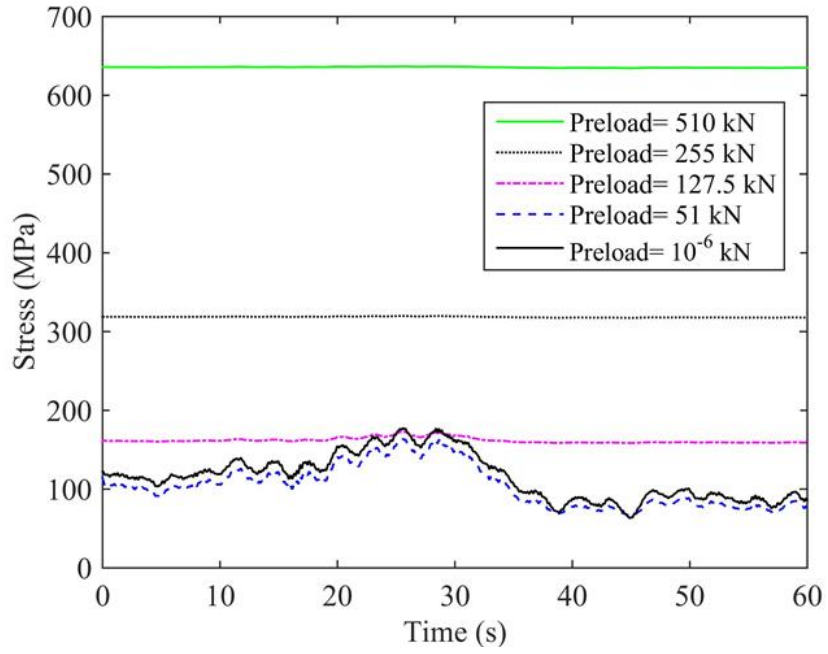

Figure 5.13. Total bolt stress for bolts with different preload levels

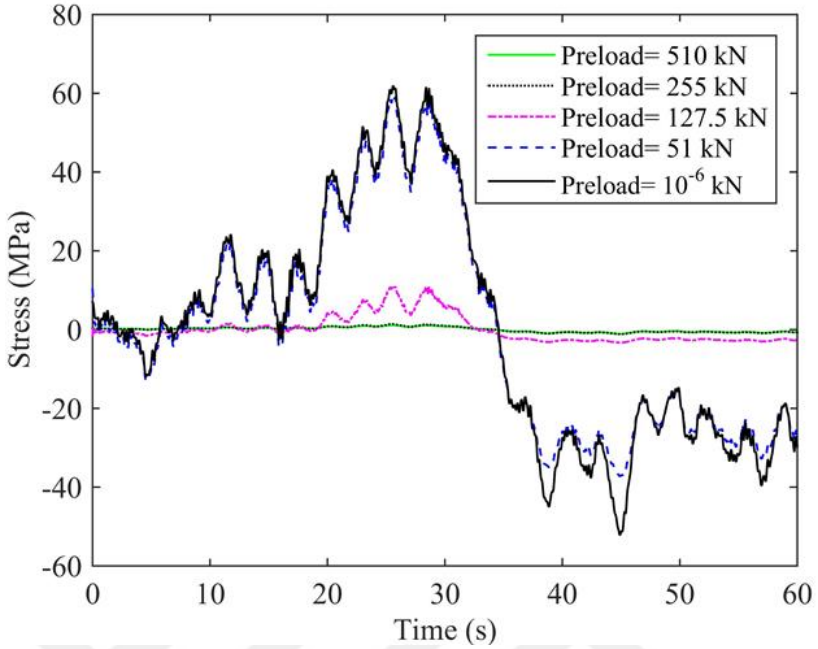

Figure 5.14. Total bolt stress, for bolts with different preload levels, averages removed

stress range histograms obtained by cycle-counting of the stress caused by axial bolt force and the total stress are shown in Figure 5.15. Taking into account of bending stresses increases the stress ranges, and therefore, the cycles move into larger stress range bins.

In Figure 5.16, the stress range histograms for multiple preload values (obtained from total stresses) are illustrated. Reduction of preload causes a shift of cycles to larger ranges, and therefore, greater fatigue damage occurs.

Miner's damage index (Eq. 4.7) explained in [6] and the mean S-N curve shown in Figure 4.24 are used in this chapter to calculate the fatigue damage. Damage index for multiple preload values accumulated in 1 min is shown in Figure 5.17. As the preload is reduced, fatigue damage increases significantly. On the other hand, including the bending stresses in the calculations changes the calculated fatigue damage greatly.

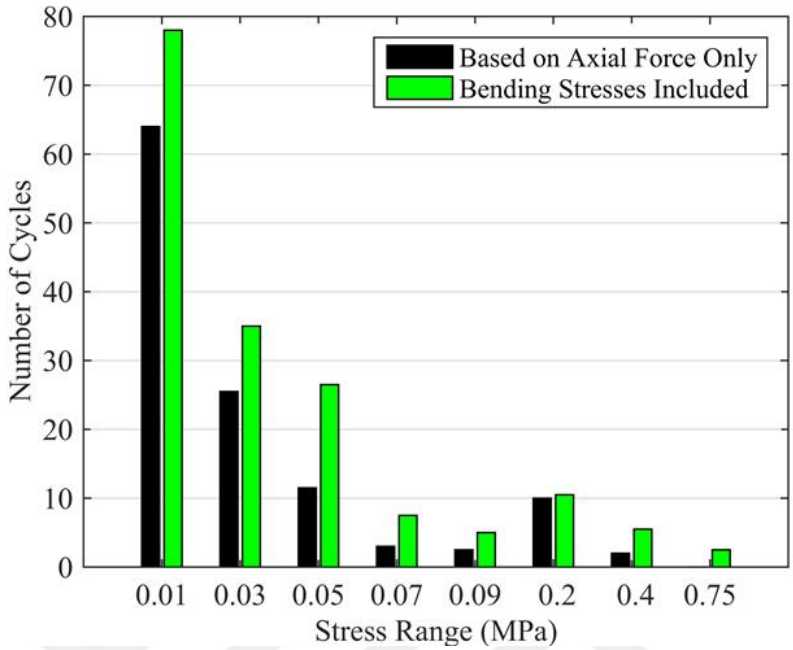

Figure 5.15. Stress range histogram for the case of bolt with 510 kN preload, stress calculated from axial force only, vs total stress

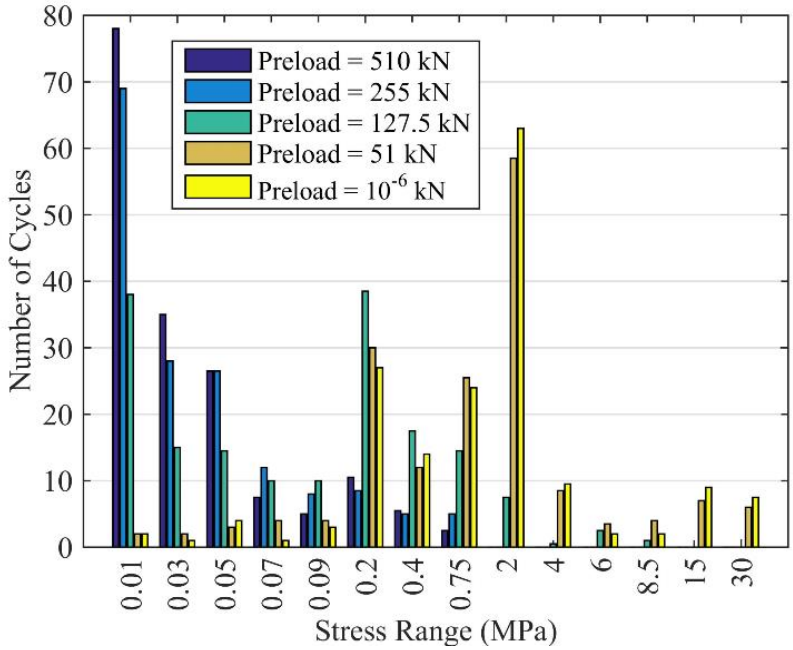

Figure 5.16. Stress range histograms obtained with different levels of bolt preload stress

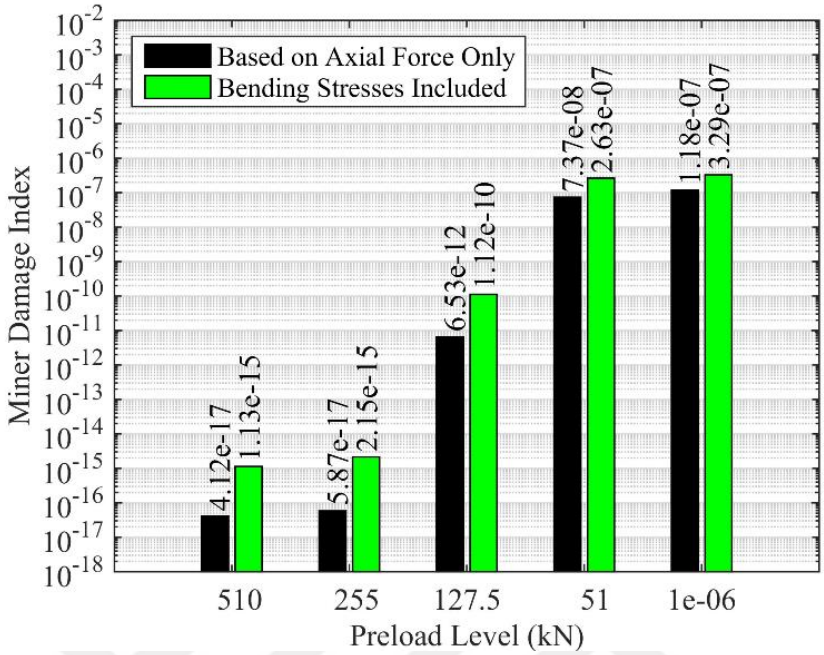

Figure 5.17. Miner's damage index obtained for different preload levels, for a 1 min loading

The results of finite element analyses as presented in this chapter showed the effect of the changing bolt preload on the extent by which the changes of external loading are transferred to the bolt. The free-body diagram of the upper half of the bolted joint of Figure 3.4 is shown in Figure 5.18. As the bolt preload is increased, the reduction in the changes of bolt force (ΔP_b) under the effect of changes of a cyclic external load (ΔP_{ex}) is compensated by an increase in the changes of contact force (resultant of contact stresses) between the flanges (ΔP_f). This can be explained by the change of the the engagement (interaction) between the flanges. To illustrate this effect, using the finite element model shown in Figure 5.4, two cases of analyses are performed. In the first case, 100 % of the design preload is applied to the bolt, and then a 40 MPa tensile stress is applied to the upper edge of the wall in the model. In the second case, 20 % of the design preload is applied to the bolt, and then the same 40 MPa tensile stress is applied to the upper edge of the wall. Contours of the contact pressure between the flanges for the two cases are shown in Figures 5.19 and 5.20. These countour plots show that under the effect of the same external loading, change

of bolt preload causes a change in the distribution of contact pressure between the flanges, which results in a change in the structural behavior of the bolted joint. In the case of the higher bolt preload (Figure 5.19), the contact pressure is concentrated near the bolt. On the other hand, in the case of a lower bolt preload value (Figure 5.20), the location of concentration of contact pressure moves towards the edge of the flange.

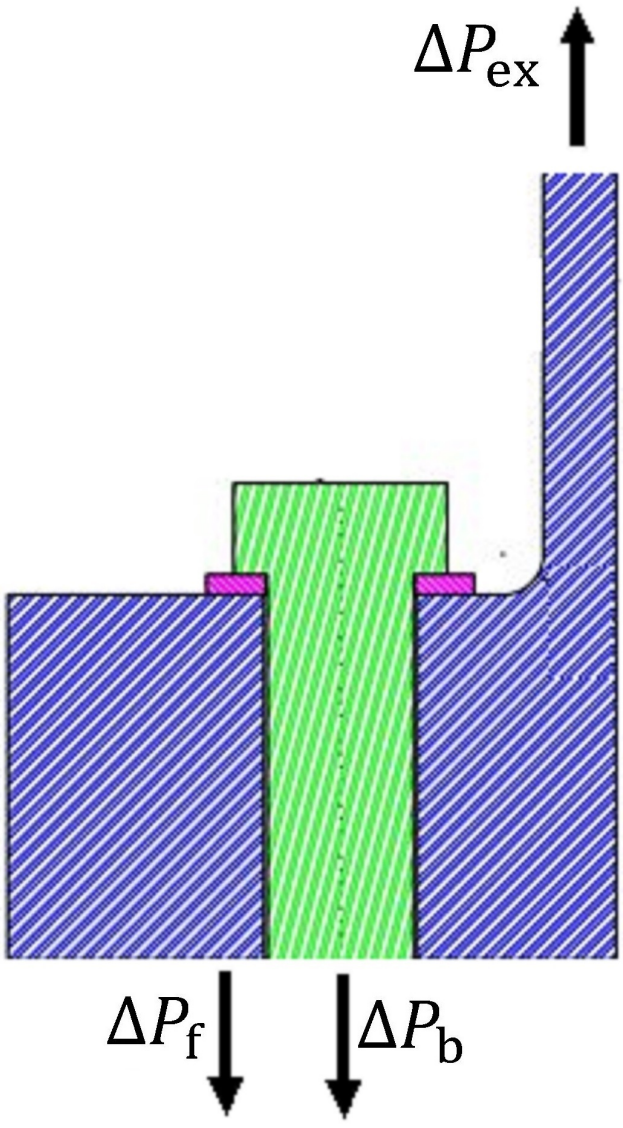

Figure 5.18. Free-body diagram of upper half of the bolted joint

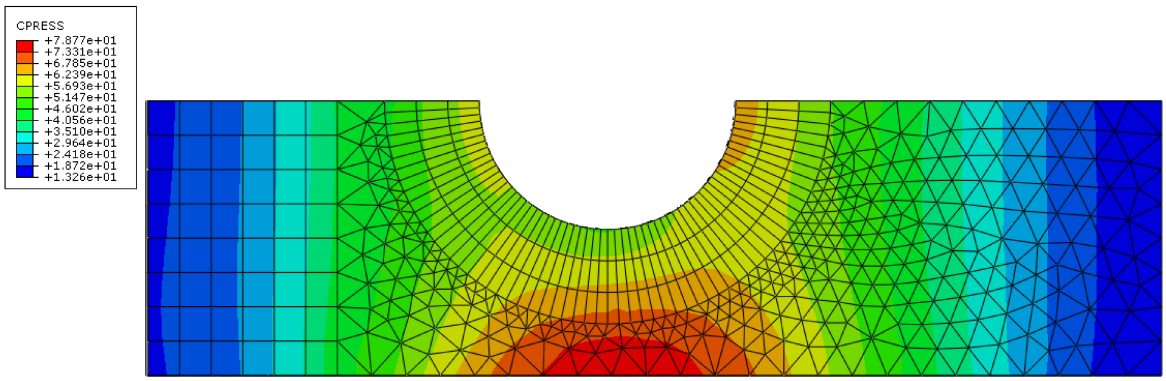

Figure 5.19. Contour of contact pressure between the flanges for the case of 100 % of bolt preload

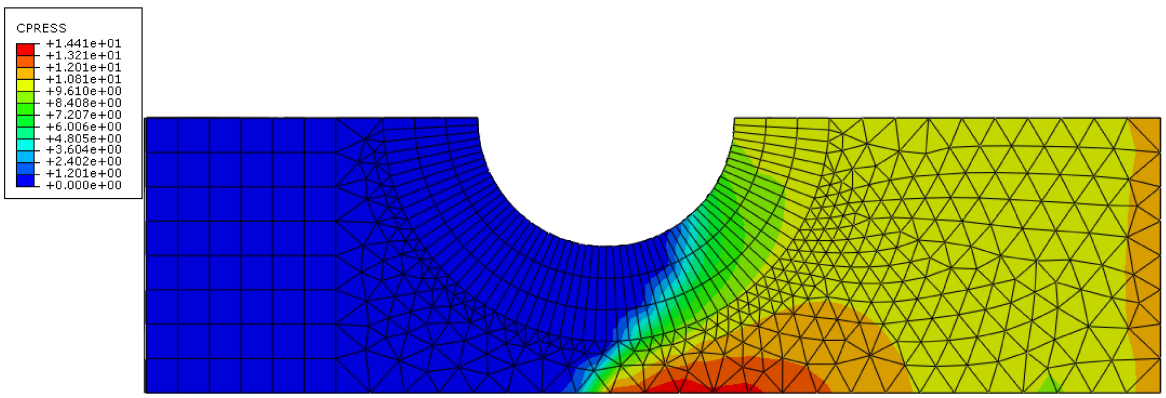

Figure 5.20. Contour of contact pressure between the flanges for the case of 20 % of bolt preload

6. CONCLUSION

A numerical procedure for estimating the fatigue lives of connection bolts of wind turbine towers is established. Uncertainties related to wind are taken into account by probability distributions of short-term average (mean) wind speed and turbulence intensity. Methods of adjusting the statistical parameters of the wind for any site based on wind speed measurements are developed. Moreover, a method is developed that provides a possibility of representing the variability of wind parameters by a set of specific values for those parameters, derived from their probability distributions.

Positions of the bolts in the connection significantly affect the demands imposed on the bolts. It Is clearly observed that the more distance each bolt has from the neutral axis of the major bending moment caused by wind, the more it is affected by the overturning moment in the connection, and thus it experiences more fatigue damage and has less fatigue life.

Fatigue lives of bolts in a wind turbine tower depend on many case-specific factors including the behavior of electro-mechanical control systems of the turbine, operational strategy of the owner, quality of construction and quality of parts. This research presents a method which is applicable for any specific wind turbine tower. Therefore, the fatigue damage estimations made in this research are intended to demonstrate how different factors and states of operation contribute to the fatigue damage in the bolts, and how they can be taken into consideration in the fatigue analysis.

The effects of bolt preload on fatigue demands on connection bolts are evaluated. Reduction of preload from 100 % to nearly 0 % results in an increase in ranges of the axial force and bending moment cycles in the bolt. Consequently, reduction of preload causes an increase in the stress ranges and fatigue damage. This effect is observed more significantly when preload is reduced to 25 %.

Inclusion of the bending stresses increases the stress ranges and the fatigue demands on the bolt greatly. This effect is observed more significantly in higher preload values.

The results of this research showed that randomness of the numerically generated wind speed time-series considerably affects the fatigue demands on the bolts. A method is presented for obtaining the probability distributions of bolt fatigue lives based on the probability distribution parameters of fatigue capacity and demand variables.

7. RECOMMENDATION FOR FUTURE WORKS

The study presented in this thesis showed the necessity of further research on the uncertainties of capacity and demand variables used in the fatigue analysis of wind turbine tower bolts. Future research on this subject can address this issue by conducting comprehensive experimental and numerical evaluations of probability distributions of the input variables used in the fatigue analysis, taking into account different operational conditions, wind parameters, quality of manufactured parts and construction practices.

REFERENCES

1. Chou, J. S. and W. T. Tu, "Failure analysis and risk management of a collapsed large wind turbine tower", *Engineering Failure Analysis*, Vol. 18, No. 1, pp. 295–313, 2011.

2. SHK, *Olycka med vindkraftverk i Lemnhult, Vetlanda kommun, Slutrapport RO 2017:01 (in Swedish)*, Statens haverikommission, Stockholm, Sweden, 2017.

3. Jonkman, J. M. and M. L. Buhl Jr, *FAST User's Guide*, National Renewable Energy Laboratory, Golden, CO, USA, 2005.

4. ABAQUS, *User's Manual*, Hibbitt, Karlsson, and Sorensen, Inc., Providence, RI, USA, 1998.

5. ASTM, *Standard practices for cycle counting in fatigue analysis, ASTM E1049-85 (Reapproved 2011)*, The American Society for Testing and Materials, West Conshohocken, PA, USA, 1997.

6. Eurocode, *Design of Steel Structures–Part 1–9: Fatigue*, European Committee for Standardization, Brussels, Belgium, 2005.

7. Ishihara, T., A. Yamaguchi, K. Takahara, T. Mekaru and S. Matsuura, "An analysis of damaged wind turbines by Typhoon Maemi in 2003", *Proceedings of the 6th Asia-Pacific Conference on Wind Engineering. Seoul, Republic of Korea*, pp. 1413–28, 2005.

8. Ciang, C. C., J. R. Lee and H. J. Bang, "Structural health monitoring for a wind turbine system: a review of damage detection methods", *Measurement Science and Technology*, Vol. 19, No. 12, p. 122001, 2008.

9. Sutherland, H. J., *On the fatigue analysis of wind turbines*, Sandia National Labs,

Albuquerque, NM, USA, 1999.

10. Ragan, P. and L. Manuel, "Comparing estimates of wind turbine fatigue loads using time-domain and spectral methods", *Wind Engineering*, Vol. 31, No. 2, pp. 83–99, 2007.

11. Ding, J. and X. Chen, "Assessing small failure probability by importance splitting method and its application to wind turbine extreme response prediction", *Engineering Structures*, Vol. 54, pp. 180–191, 2013.

12. Do, T. Q., J. W. van de Lindt and H. Mahmoud, "Fatigue life fragilities and performance-based design of wind turbine tower base connections", *Journal of Structural Engineering*, Vol. 141, No. 7, p. 04014183, 2015.

13. Do, T. Q., H. Mahmoud and J. W. van de Lindt, "Fatigue life of wind turbine tower bases throughout Colorado", *Journal of Performance of Constructed Facilities*, Vol. 29, No. 4, p. 04014109, 2015.

14. Swartz, R. A., J. P. Lynch, S. Zerbst, B. Sweetman and R. Rolfes, "Structural monitoring of wind turbines using wireless sensor networks", *Smart Structures and Systems*, Vol. 6, No. 3, pp. 183–196, 2010.

15. Benedetti, M., V. Fontanari and D. Zonta, "Structural health monitoring of wind towers: remote damage detection using strain sensors", *Smart Materials and Structures*, Vol. 20, No. 5, p. 055009, 2011.

16. Pollino, M. C. and A. A. Huckelbridge, "In-situ measurements of fatigue demands on a wind turbine support structure", *2012 IEEE Energytech*, pp. 1–5, IEEE, 2012.

17. Benedetti, M., V. Fontanari and L. Battisti, "Structural health monitoring of wind towers: residual fatigue life estimation", *Smart Materials and Structures*, Vol. 22, No. 4, p. 045017, 2013.

18. Shirani, M. and G. Härkegård, "Fatigue life distribution and size effect in ductile cast iron for wind turbine components", *Engineering Failure Analysis*, Vol. 18, No. 1, pp. 12–24, 2011.

19. Shirani, M. and G. Härkegård, "Large scale axial fatigue testing of ductile cast iron for heavy section wind turbine components", *Engineering Failure Analysis*, Vol. 18, No. 6, pp. 1496–1510, 2011.

20. Ernst, B. and J. R. Seume, "Investigation of site-specific wind field parameters and their effect on loads of offshore wind turbines", *Energies*, Vol. 5, No. 10, pp. 3835–3855, 2012.

21. Mao, W. and Z. Zhou, "Ground effects on wind-induced responses of a closed box girder", *Wind and Structures*, Vol. 25, No. 4, pp. 397–413, 2017.

22. Ilhan, A., M. Bilgili and B. Sahin, "Analysis of aerodynamic characteristics of 2 MW horizontal axis large wind turbine", *Wind and Structures*, Vol. 27, No. 3, pp. 187–197, 2018.

23. GL, *Guideline for the Certification of Wind Turbines*, Germanischer Lloyd, Hamburg, Germany, 2010.

24. IEC, *Wind Turbines Part 1: Design Requirements*, International Electrotechnical Commission, Geneva, Switzerland, 2005.

25. Robinson, C., E. Paramasivam, E. Taylor, A. Morrison and E. Sanderson, *Study and Development of a Methodology for the Estimation of the Risk and Harm to Persons From Wind Turbines, RR968 Research Report*, Health and Safety Executive, Bootle, Merseyside, UK, 2013.

26. Heistermann, C., W. Husson and M. Veljkovic, "Flange connection vs. friction connection in towers for wind turbines", *Nordic Steel and Construction Conference; Stålbyggnadsinstitutet: Stockholm, Sweden*, pp. 296–303, 2009.

27. Pavlović, M., C. Heistermann, M. Veljković, D. Pak, M. Feldmann, C. Rebelo and L. S. da Silva, "Friction connection vs. ring flange connection in steel towers for wind converters", *Engineering Structures*, Vol. 98, pp. 151–162, 2015.

28. Seidel, M. and P. Schaumann, "Measuring Fatigue Loads of Bolts in Ring Flange Connections", *EWEC-CONFERENCE*, pp. 255–258, 2001.

29. Hamdi, H. and K. Farah, "Beam finite element model of a vibrate wind blade in large elastic deformation", *Wind and Structures*, Vol. 26, No. 1, pp. 25–34, 2018.

30. Schaumann, P., R. Eichstädt *et al.*, "Fatigue assessment of high-strength bolts with very large diameters in substructures for offshore wind turbines", *The Twenty-fifth International Ocean and Polar Engineering Conference*, International Society of Offshore and Polar Engineers, 2015.

31. Oechsner, M., J. Beyer, F. Simonsen, P. Schaumann and R. Eichstädt, "Experimental and analytical assessment of the fatigue strength of bolts with large dimensions under consideration of boundary layer effects", *METEC & 2nd European steel technology and application days (Düsseldorf, Germany)*, pp. 1–6, 2015.

32. Van-Long, H., J. Jean-Pierre and D. Jean-François, "Behaviour of bolted flange joints in tubular structures under monotonic, repeated and fatigue loadings I: Experimental tests", *Journal of Constructional Steel Research*, Vol. 85, pp. 1–11, 2013.

33. Blachowski, B. and W. Gutkowski, "Effect of damaged circular flange-bolted connections on behaviour of tall towers, modelled by multilevel substructuring", *Engineering Structures*, Vol. 111, pp. 93–103, 2016.

34. Williams, J., R. Anley, D. Nash and T. Gray, "Analysis of externally loaded bolted joints: Analytical, computational and experimental study", *International Journal of Pressure Vessels and Piping*, Vol. 86, No. 7, pp. 420–427, 2009.

35. Pedersen, N. L. and P. Pedersen, "Stiffness analysis and improvement of bolt-plate contact assemblies", *Mechanics Based Design of Structures and Machines*, Vol. 36, No. 1, pp. 47–66, 2008.

36. Pedersen, N. L. and P. Pedersen, "On prestress stiffness analysis of bolt-plate contact assemblies", *Archive of Applied Mechanics*, Vol. 78, No. 2, pp. 75–88, 2008.

37. Badrkhani Ajaei, B. and S. Soyoz, "Analytical and experimental fatigue analysis of wind turbine tower connection bolts", *Wind and Structures*, Vol. 31, No. 1, pp. 1–14, 2020.

38. Lu, C., Q. Li, S. Huang, A. Y. Tuan, L. Zhi and S. C. Su, "Evaluation of wind loads and wind induced responses of a super-tall building by large eddy simulation", *Wind and Structures*, Vol. 23, No. 4, pp. 313–350, 2016.

39. Gol-Zaroudi, H. and A. M. Aly, "Open-jet boundary-layer processes for aerodynamic testing of low-rise buildings", *Wind and Structures*, Vol. 25, No. 3, pp. 233–259, 2017.

40. Elshaer, A., G. Bitsuamlak and H. Abdallah, "Variation in wind load and flow of a low-rise building during progressive damage scenario", *Wind and Structures*, Vol. 28, No. 6, pp. 389–404, 2019.

41. Ke, S., W. Yu, T. Wang, L. Zhao and Y. Ge, "Wind loads and load-effects of large scale wind turbine tower with different halt positions of blade", *Wind and Structures*, Vol. 23, No. 6, pp. 559–575, 2016.

42. Gunter, W. S., J. L. Schroeder, C. C. Weiss and E. C. Bruning, "Surface measurements of the 5 June 2013 damaging thunderstorm wind event near Pep, Texas", *Wind and Structures*, Vol. 24, No. 2, pp. 185–204, 2017.

43. Jonkman, B. J. and L. Klicher, *TurbSim User's Guide: Version 1.06*, National

Renewable Energy Laboratory, Golden, CO, USA, 2012.

44. Hanbay, S., *Vibration-Based Structural Health Monitoring of a Wind Turbine Incorporating Environmental and Operational Conditions*, M.Sc. Thesis, Bogazici University, Istanbul, Turkey., 2019.

45. Eurocode, *Design of Steel Structures–Part 1–1: General Rules for Buildings*, European Committee for Standardization, Brussels, Belgium, 2005.

46. DNVGL, *Fatigue Design of Offshore Steel Structures*, Det Norske Veritas Germanischer Lloyd, Oslo, Norway, 2016.

47. DNVGL, *Support Structures for Wind Turbines*, Det Norske Veritas Germanischer Lloyd, Oslo, Norway, 2016.

48. Nowak, A. S. and K. R. Collins, *Reliability of Structures*, McGraw-Hill, USA, 2000.

49. Abernethy, R. B., *The New Weibull Handbook: Reliability and Statistical Analysis for Predicting Life, Safety, Supportability, Risk, Cost and Warranty Claims*, Society of Automotive Engineers, Warrendale, PA, USA, 1998.

50. Badrkhani Ajaei, B. and S. Soyoz, "Effects of preload deficiency on fatigue demands of wind turbine tower bolts", *Journal of Constructional Steel Research*, Vol. 166, p. 105933, 2020.

51. Abasolo, M., J. Aguirrebeitia, R. Avilés and I. Fernández de Bustos, "A tetraparametric metamodel for the analysis and design of bolting sequences for wind generator flanges", *Journal of Pressure Vessel Technology*, Vol. 133, No. 4, 2011.

52. Nagata, S., T. Sawa and S. Hamamoto, "Effects of Scatter in Bolt Preload on the Sealing Performance in Bolted Flange Connections with Cover of Pressure Vessel under Internal Pressure", *ASME 2006 Pressure Vessels and Piping/ICPVT-11 Conference*, pp. 241–246, American Society of Mechanical Engineers Digital

Collection, 2006.

53. Chen, A., C. Schaeffer, Y. Zhang, B. Phares, B. Shafei, M. Yang, Z. Lin and S. Paudel, *Re-tightening the Large Anchor Bolts of Support Structures for Signs and Luminaires*, Minnesota Department of Transportation, Saint Paul, MN, USA, 2018.

54. Liu, J., H. Ouyang, J. Peng, C. Zhang, P. Zhou, L. Ma and M. Zhu, "Experimental and numerical studies of bolted joints subjected to axial excitation", *Wear*, Vol. 346, pp. 66–77, 2016.

55. Hobbs, J., R. Burguete, P. Heyes and E. Patterson, "The effect of eccentric loading on the fatigue performance of high-tensile bolts", *International Journal of Fatigue*, Vol. 22, No. 6, pp. 531–538, 2000.

56. Couchaux, M., M. Hjiaj, I. Ryan and A. Bureau, "Effect of contact on the elastic behaviour of tensile bolted connections", *Journal of Constructional Steel Research*, Vol. 133, pp. 459–474, 2017.

57. Huang, F., D. Zhang, W. Hong and B. Li, "Mechanism and calculation theory of prying force for flexible flange connection", *Journal of Constructional Steel Research*, Vol. 132, pp. 97–107, 2017.

58. DNV-OS-C101, *Design of Offshore steel Structures, General (LRFD Method)*, Det Norske Veritas (DNV), Oslo, Norway, 2011.

59. Gorst, N. J. S., S. J. Williamson, P. F. Pallett and L. A. Clark, *Friction in TemporaryWorks (Research Report 071)*, Health and Safety Executive (HSE), Birmingham, UK, 2003.

60. Huang, W. and X. Zhang, "Wind field simulation over complex terrain under different inflow wind directions", *Wind and Structures*, Vol. 28, No. 4, pp. 239–253, 2019.

61. Mirfazli, S. K., M. H. Giahi and A. J. Dehkordi, "Numerical optimization of a vertical axis wind turbine: case study at TMU campus", *Wind and Structures*, Vol. 28, No. 3, pp. 191–201, 2019.

62. Ahmed, A., S. Ahmad and J. Reshi, "Bayesian analysis of Rayleigh distribution", *International Journal of Scientific and Research Publications*, Vol. 3, No. 10, pp. 1–9, 2013.

APPENDIX A: ESTIMATION OF LONG-TERM AVERAGE OF WIND SPEED

Wind speeds are recorded by an ultrasonic device of the weather station at 60 m height from ground. However, for aerodynamic simulations of the wind turbine, wind speeds at the hub height (55 m) are needed. The Power-Law described by [43, 60, 61] and given in Eq. A.1 is used for correcting the wind speeds for hub height.

$$u_{hub} = u_{measurement} \left(\frac{h_{hub}}{h_{measurement}} \right)^{m} \tag{A.1}$$

where, $h_{measurement} = 60$ m is the height of the measurement device, $u_{measurement}$ is the wind speed measured by the device, h_{hub} is the height of the turbine hub, u_{hub} is the wind speed at hub height, and m is the exponent for the Power-Law, for which an average value of $m = 0.2$ is assumed here according to [43].

In order to estimate the long-term average of wind speed (V_{ave}) based on the recorded wind speed measurements, a method suggested by [62] is used. According to [62], for a random variable x which has a Rayleigh distribution with the PDF given by Eq. A.2, the parameter η of the distribution can be estimated by the value $\hat{\eta}$ given by Eq. A.3.

$$f_R(X) = \frac{X}{\eta^2} \exp\left(\frac{-X^2}{2\eta^2} \right) \tag{A.2}$$

$$\hat{\eta} = \frac{\Gamma\left(\frac{2n-1}{2}\right)}{\Gamma(n)} \sqrt{\frac{\sum_{i=1}^{n} X_i^2}{2}} \tag{A.3}$$

where, X_i are the n values of the sample of observations of the random variable X, and Γ is the gamma function. Therefore, for the PDF of V_a given by Eq. (2), the

parameter V_{ave} is estimated by the value $\hat{V}_{ave}$ given by Eq. A.4:

$$\hat{V}_{ave} = \sqrt{\frac{\pi}{2}} \frac{\Gamma\left(\frac{2n-1}{2}\right)}{\Gamma(n)} \sqrt{\frac{\sum_{i=1}^{n} V_{ai}^2}{2}} \tag{A.4}$$

where V_{ai} are the $n = 277$ values of the sample of observations of the random variable V_a.

APPENDIX B: ESTIMATION OF MEAN AND STANDARD DEVIATION OF TURBULENCE INTENSITY

In Figure B.1, the linear relationship (Eq. 4.3) suggested for mean of σ_V by [24] is shown by a dotted line. The scattered dots show σ_V vs V_a pairs of individual measurements by the weather station between 2015/04/01, 0:00 and 2015/04/02, 23:50. Measurements are converted to wind speed at hub height, using Eq. A.1. It is clearly observed from Figure B.1 that the relationship suggested by [24] (Eq. 4.3) overestimates the mean of σ_V for each value of V_a . Therefore, in this research $\mu_{\sigma_V|V_a}$ (mean of σ_V for any specific value of V_a) is calculated by a linear relationship shown in Figure B.1 by a solid line fitted to the measurements by a regression analysis.

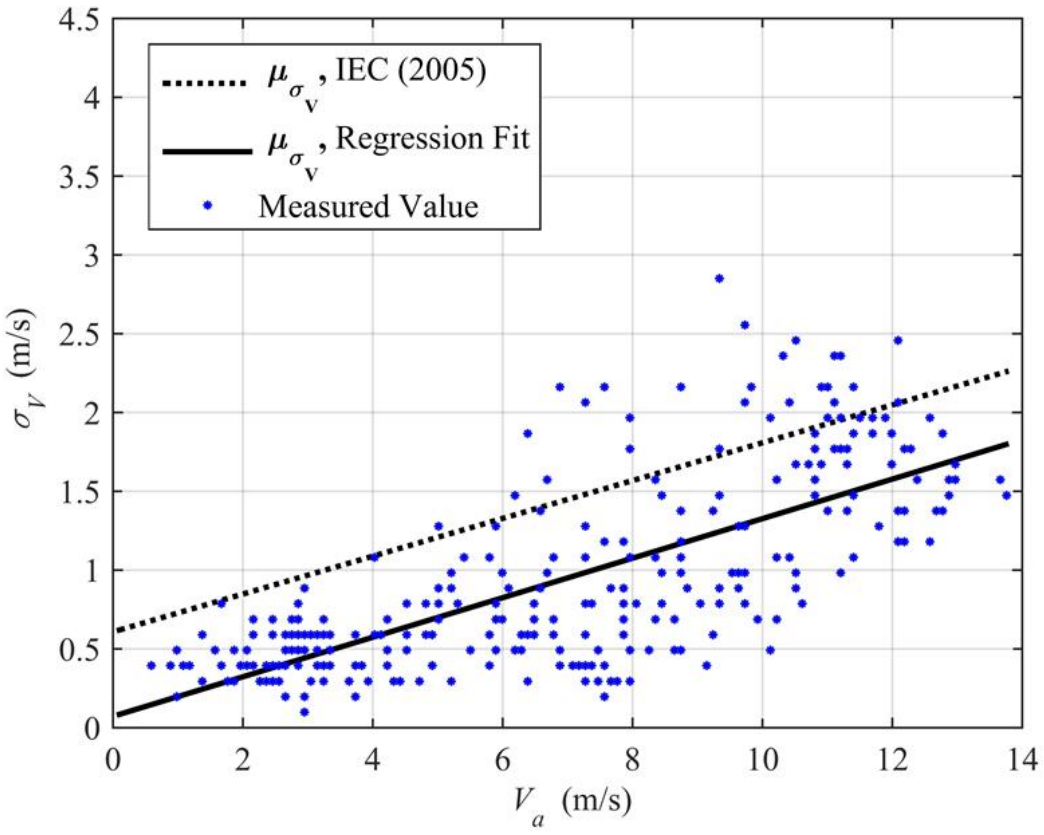

Figure B.1. Adjusting the linear relationship for mean of σ_V

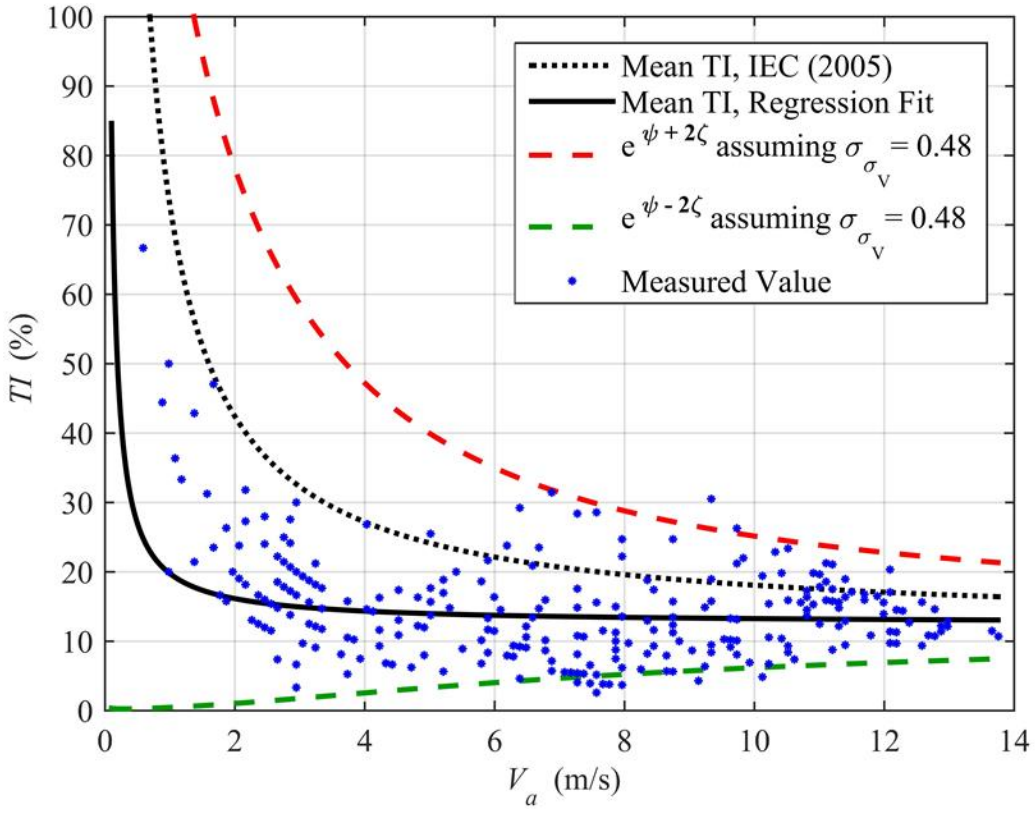

Figure B.2. Adjusting the standard deviation of σ_V

According to Eq. 4.1, for every given value of V_a, TI is equal to the log-normally distributed random variable σ_V divided by a constant V_a. Therefore, TI is also log-normally distributed, and based on the rules governing the linear functions of random variables [48] has mean and standard deviation values given by Eqs. B.1 and B.2.

$$\mu_{TI|V_a} = \frac{\mu_{\sigma_V|V_a}}{V_a} \tag{B.1}$$

$$\sigma_{TI|V_a} = \frac{\sigma_{\sigma_V|V_a}}{V_a} \tag{B.2}$$

Figure B.2 shows the variations of TI for different values of V_a. The dotted line represents the suggestion of [24] (According to Eqs. 4.3 and B.1), the solid line is obtained by dividing the regression line of Figure B.1 by the V_a axis values, according to Eq. B.1, and the scattered dots show the same individual measurements as shown in Figure B.1. Since TI has a log-normal probability distribution, $\mathrm{Ln}(TI)$ has a normal probability distribution with the mean and standard deviation denoted by ψ and ζ respectively. Therefore, 95.4% of $\mathrm{Ln}(TI)$ values should be inside the interval $\psi - 2\zeta \leq \mathrm{Ln}(TI) \leq \psi + 2\zeta$. As a result, 95.4% of TI values should be inside the interval $e^{\psi-2\zeta} \leq TI \leq e^{\psi+2\zeta}$. The upper and lower limits of this interval are plotted as dashed envelope curves in Figure B.2. The right hand side of Eq. 4.4 suggested by [24] for σ_{σ_V} (standard deviation of σ_V) is changed here to a value of 0.48 in order to have 95.4% of measurements inside the two envelope curves. Based on the adjustments made above and using Eqs. B.1 and B.2, in this research, for any specific value of V_a, mean and standard deviation of TI are calculated using Eqs. 4.5 and 4.6.